The Impact of Explosive Volcanic Eruptions on the North Atlantic Climate System



Helena Cotterill

Brasenose College

University of Oxford

This thesis is submitted for the degree of

Master of Science by Research

Hilary Term 2021

Declaration of Authorship:

I confirm that the work presented here is entirely my own. I carried out the analysis as described in this thesis and produced the figures included, except where clearly stated in the figure caption.

I confirm that none of this work is being considered for another degree or qualification.

Acknowledgements

The very final part of the thesis to write, and then it's finally finished! There are so many people I am thankful for who have been there during the (long, long) time it has taken me to work on this. There have been many twists and turns over the years, and who ever thought I'd be writing most of this during a lockdown caused by a global pandemic? Despite everything, you have all stuck around, so here I'll say a short thank you to as many as I can.

First and foremost, my supervisor: Lesley Gray. Thank you for the opportunity for me to work with you, and thank you for your help, support, and patience throughout the last few years – this would not have been finished without you.

Next, to the other people who have shared office 113 over the years, but especially Matt for generally putting up with me singing and getting far too into our chats about rollercoasters, and also allowing me to distract you with the latest outreach thing I was planning, and Verena for many excellent chats about life and everything else over a glass of wine.

Speaking of outreach, I have to thank the Physics outreach team – you are all superstars, and I would not be where I am today without all of you! Kathryn, for trusting me to take over your role and helping me learn so much about the world of outreach and Quantum Materials. Chris and Sian for giving me the job in the first place and supporting me throughout. Ollie for being a fantastic cover for Sian – it was lovely to have someone else starting at the same time as me so we could help each other learn the ropes! And especially Lena for dragging me into the world of outreach in the first place and from there becoming a life-long friend.

My original Oxford Physics (+ Egyptologist) gang – even though we have all ended up in slightly different places now, I love that we still all come together whenever we can, even if it is via Zoom! And to those who also stuck around in Oxford: Amy, Rory, Ellie, and Aidan. I miss you all dearly and can't wait until we can gather and eat take out and play D&D again like the nerds we are.

The ever-changing members of OUGSS who I have come to know over the years, and who have all joined me in prancing about on stage singing Victorian Operetta – you are all mad, just like me, and I love you all! Special shout out goes to three amazing American ladies: Gabrielle for always having my back with a Facetime call even being an ocean away, Chloe for helping me actually sit down and write this thing (I miss our study dates) and sharing a love for gin and singing vicariously, and forever my partner in crime Aversa for always being there for me throughout all my endeavours, musical and otherwise. I miss you all and I hope we can end up on the same continent again sometime soon. And for those of you who ARE in the same country as me, I can't wait until we can all meet for a good natter over a drink in the park again – socially distanced, of course – and eventually share the stage with you all again!

Finally, to my family. Grandad, who will forever be my biggest fan. Gran for always being up for a good rant about the state of the world. And my mum – you really are the Lorelai to my Rory, and I don't know what I would do without you. (And I can't forget my cat, Casper, for keeping me company at home and making sure to scream at me when I've been working too long!) I love you all so much and am so grateful for your support, now and always.

To all those mentioned here, and everyone else I am so happy to call my friend, I am eternally grateful – thank you.

Abbreviations used in this thesis:

20CR	Twentieth Century Reanalysis
AGP	Absolute Geopotential Height
AO	Arctic Oscillation
AMO	Atlantic Multidecadal Oscillation
AMOC	Atlantic Meridional Overturning Circulation
CMIP	Coupled Model Intercomparison Project
DJF	December-January-February
DVI	Dust Veil Index
EA	East Atlantic
ECMWF	European Centre for Medium-range Weather Forecasting
EOF	Empirical Orthogonal Function
EnKF	Ensemble Kalman Filter
ENSO	El Niño-Southern Oscillation
GCM	General Circulation Model
HadISST	Hadley Centre Sea Ice and Sea Surface Temperature
HadSLP	Hadley Centre Sea Level Pressure
IR	Infrared
IVI	Ice Core Volcanic Index
NAO	North Atlantic Oscillation
NAM	Northern Annular Mode
NCAR	National Center for Atmospheric Research
NCEP	National Centers for Environmental Prediction
NH	Northern Hemisphere
NOAA	National Oceanic and Atmospheric Administration
QBO	Quasi-Biennial Oscillation

SLP	Sea level pressure
SST	Sea surface temperature
SSW	Sudden Stratospheric Warming
u	Zonal Wind
UV	Ultraviolet
VEI	Volcanic Explosivity Index
Z500	500hPa Geopotential Height

Contents

Abstract 9

Section 1: Introduction 10

Section 2: Background 12

2.1 The Atmosphere 13

2.1.1 Atmospheric Structure 13

2.1.2 Atmospheric Circulation 15

2.2 Volcanic Eruptions 18

2.2.1 Radiative Effects 21

2.2.2 Dynamical Effects 23

2.2.3 Impact on Ozone 27

2.2.4 Modelling the Impacts of Volcanic Eruptions 27

2.2.5 Link to and Impact on ENSO..... 29

2.2.6 Long Term Impacts & the Effect of Volcanic Eruptions on the Oceans .. 31

2.3 Summary and Thesis Objectives 33

Section 3: Data & Methodology 34

3.1 Multiple Linear Regression 34

3.2 Volcanic Indices 39

3.3 Other Regression Indices 41

3.4 Volcanic Eruptions & Regression Periods 42

3.5 Analysed Data 44

3.5.1 Observational Data 44

a. Sea Level Pressure 47

b. Sea Surface Temperatures 47

c. NAO 47

3.5.2 Reanalysis Data 48

a. SLP & SSTs 51

b. North Atlantic Jet 51

c. Blocking 52

Section 4: Results & Analysis 54

4.1 Sea Level Pressure 54

4.1.1 Regression Analysis 54

4.1.2 Composite Analysis 61

4.2 Sea Surface Temperature 65

4.3 The Nao & the North Atlantic Jet 70

4.3.1 The NAO Index 70

4.3.2 Jet Latitude & Speed 72

4.3.3 850hPa Zonal Winds 76

4.4 Blocking 78

Section 5: Summary & Further Work 81

5.1 Further Work 83

References 86

Abstract:

Volcanic eruptions have a variety of impacts on the climate, from short-term reductions in temperature lasting only days, to longer term impacts due to the influence of stratospheric aerosols lasting 2-3 years, and even decadal scale effects arising from the impact on the oceans. Large tropical eruptions have the biggest impact on the stratosphere and have the potential to have long lasting global impacts. These large eruptions allow sulphate aerosols to be formed within the tropical stratosphere and transported globally by the stratospheric circulation, not only causing the well-known global averaged surface cooling, but also heating within the stratosphere due to the aerosols which can cause significant dynamical feedbacks.

In this thesis, I investigate the impact of such large tropical eruptions on the North Atlantic wintertime climate. I analyse observational and reanalysis datasets for periods within 1870-2010 using multiple linear regression to try to isolate the volcanic response from other forms of climate variability in sea level pressure (SLP), sea surface temperature (SST), the North Atlantic jet latitude and speed, and atmospheric blocking. I do this at various lags from 0 to 5 years following an eruption, which shows the initial wintertime surface response similar to a positive North Atlantic Oscillation (NAO) phase as found in previous studies. However, the strongest signal appears during the first winter and doesn't persist as strongly into the second as these studies have suggested. Focusing on time periods centred on specific eruptions shows the strongest response comes from the Mount Pinatubo eruption of 1991, and that the eruption of Agung in 1963 shows a very different response pattern. A 'lag 4 response' also appears during the 5th post-eruption winter in several fields, which, if real, could suggest the influence of other mechanisms, possibly involving the ocean, and warrants further investigation.

1. Introduction

Volcanic eruptions have many different and significant impacts on the weather and climate, with timescales lasting from hours or days, to years, and even decades. In the short term, this includes reductions in surface temperature and the diurnal cycle, which can last for a few days. Longer term impacts due to stratospheric aerosols resulting from an eruption can persist for up to two or three years and can influence the climate through both radiative and dynamical processes. On even longer timescales, decadal and multidecadal scale effects have been reported, particularly when considering the impact of an eruption upon the oceans and the resulting feedbacks.

Especially strong volcanic eruptions occurring in equatorial latitudes have the largest impact on the stratosphere, since it is in these locations where any gases emitted during an eruption have the strongest chance of being lofted higher in the atmosphere due to strong vertical convection. From here, the resulting aerosol cloud can be advected around the globe, having the potential to influence the global climate, not just a localised region.

While a great deal of research is directed at understanding and modelling the nature of the emitted aerosol and its radiative impacts, less attention had been directed at looking into the dynamical impacts of these strong tropical eruptions and the mechanisms involving the stratosphere. Being able to fully understand all these impacts and model these as accurately as possible would be of great importance should a similarly large eruption occur again in the future.

In this thesis, I present analysis of the volcanic signals present in different observational and reanalysis datasets. I use a multiple linear regression analysis method to try to separate out the volcanic influence from other sources of climate variability, including (but not limited to) the 11-year solar cycle, the El Nino-Southern Oscillation (ENSO), and the Atlantic Multidecadal Oscillation (AMO). I focus on the wintertime December-January-February (DJF) averaged period

over the North Atlantic sector to investigate the impacts involving the stratosphere and the polar vortex. In particular, I analyse the volcanic signal in mean sea level pressure (SLP) and sea surface temperature (SST), as well as diagnostics representing the North Atlantic jet, in terms of both latitude and speed of the jet, and atmospheric blocking events.

I show that, in general, there is consistency between observational and reanalysis data, and there is also a good degree of consistency with previous studies, however I show that the strongest signal appears to be coming from the first winter immediately following an eruption and doesn't persist into the second winter as significantly as has been reported in previous studies. I also show that focusing on smaller time periods centred on individual large eruptions shows greatly differing behaviour between certain eruptions, most significantly the eruptions of Mount Pinatubo in 1991 and Agung in 1963. I further show that a lagged response appearing in the 5th winter (a 'lag 4 response') appears significantly in several fields, which would benefit from further study to fully confirm whether this is a real response, and if so what mechanisms are involved.

An introduction to the range of impacts volcanic eruptions have on the climate is given in Section 2, along with a brief overview of the atmosphere in terms of its structure and large-scale circulation, and a discussion of previous modelling studies which focus on modelling the impact of these eruptions. In Section 3, I describe the datasets and methodology used, and I present the results of my analysis along with a discussion of these results in Section 4. Section 5 then summarises the conclusions from this work and the possible direction of future work in light of these findings.

2. Background

The focus of this thesis will be especially strong tropical volcanic eruptions and the impact these have on the surface climate due to dynamical mechanisms involving the stratosphere. Such mechanisms and other radiative impacts of volcanic eruptions are introduced and discussed in this section.

To introduce these eruptions, Figure 1 shows a map of the largest volcanic eruptions since the 19th century illustrating both their location and their size based on the Volcanic Explosivity Index (VEI; see Section 3.2). Some of the largest such eruptions, and the focus of both this thesis and many other studies in this area, are namely:

- Krakatau, Indonesia, 1883
- Santa Maria, Guatemala, 1902
- Mt. Agung, Indonesia, 1963
- El Chichón, Mexico, 1982
- Mount Pinatubo, Philippines, 1991

These eruptions, along with a few smaller but still relatively explosive eruptions since 1870, are the focus of discussion here. Further details of these eruptions can be found in Section 3 in Table 1. It is eruptions such as these which are both explosive and located in equatorial latitudes which have the greatest impact on the stratosphere. This is due to both the amount of volcanic aerosols emitted during the eruption and the atmospheric circulation at these locations. Why this is the case is further discussed below.

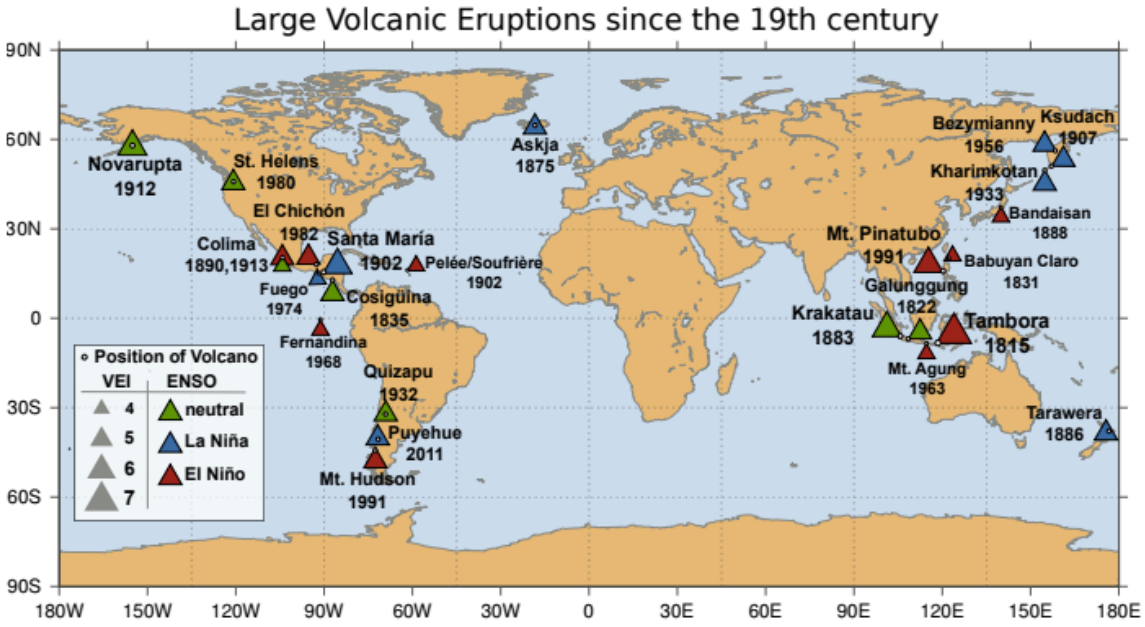


Figure 1: Reproduced from Wunderlich and Mitchell (2017; Figure 1) – a map of the large volcanic eruptions since the 19th century. The size of the triangle gives the volcanic explosivity index (VEI) and the colour indicates the ENSO phase in the 1st winter following the eruption.

2.1 The Atmosphere

To understand the full impact volcanic eruptions have on our climate, we first need to introduce the structure and circulation within the atmosphere. However, the atmosphere is well known to be a very complicated system with many different elements and influences all at play and affecting each other. The consequences of a volcanic eruption are only one part of this and are also heavily influenced by all the other influences and feedbacks. Here, I will briefly introduce the relevant aspects of the atmosphere and its dynamics before moving on to discuss the impacts of volcanic eruptions.

2.1.1 Atmospheric Structure

The vertical structure of the atmosphere is divided into layers largely based on its vertical temperature profile, as shown in Figure 2. The region of the atmosphere closest to the surface is known as the troposphere and corresponds to where the global average temperature

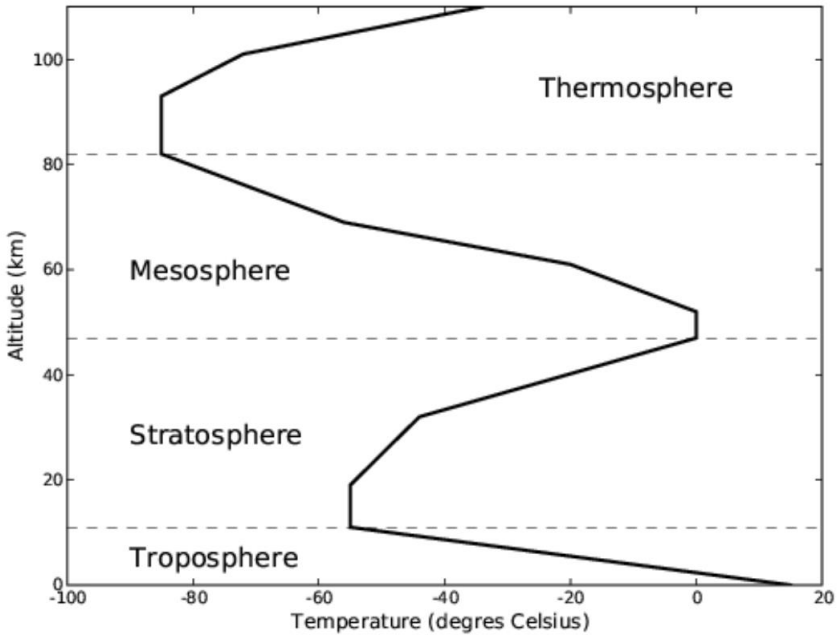


Figure 2: The approximate vertical temperature profile of the atmosphere and the corresponding structural layers. Figure taken from: https://commons.wikimedia.org/wiki/File:Profil_temperature_atmosphere.png

decreases with height. It is in this region that the majority of what we call 'weather' occurs and has the most obvious direct impacts on human activity and society wellbeing. The next layer up is known as the stratosphere, with the region between here and the troposphere below known as the tropopause, shown in Figure 2 as the region of near constant temperature. The tropopause varies in height based on latitude, with an average height of 17km at the equator, decreasing to around 9km over the poles (Hoinka 1999). Above this tropopause lies the stratosphere where the temperature actually increases with height. This region extends to a height of around 50km. Above the stratosphere is the mesosphere where the temperature again decreases with height.

Although the stratosphere may not have 'weather' in the way we usually describe it in the troposphere, it still shows a wide range of dynamical behaviour, some of which can indeed influence the weather and climate through links down to the troposphere, the mechanisms of these still being widely explored (e.g. Baldwin and Dunkerton, 2001, or Kidston et al., 2015). It

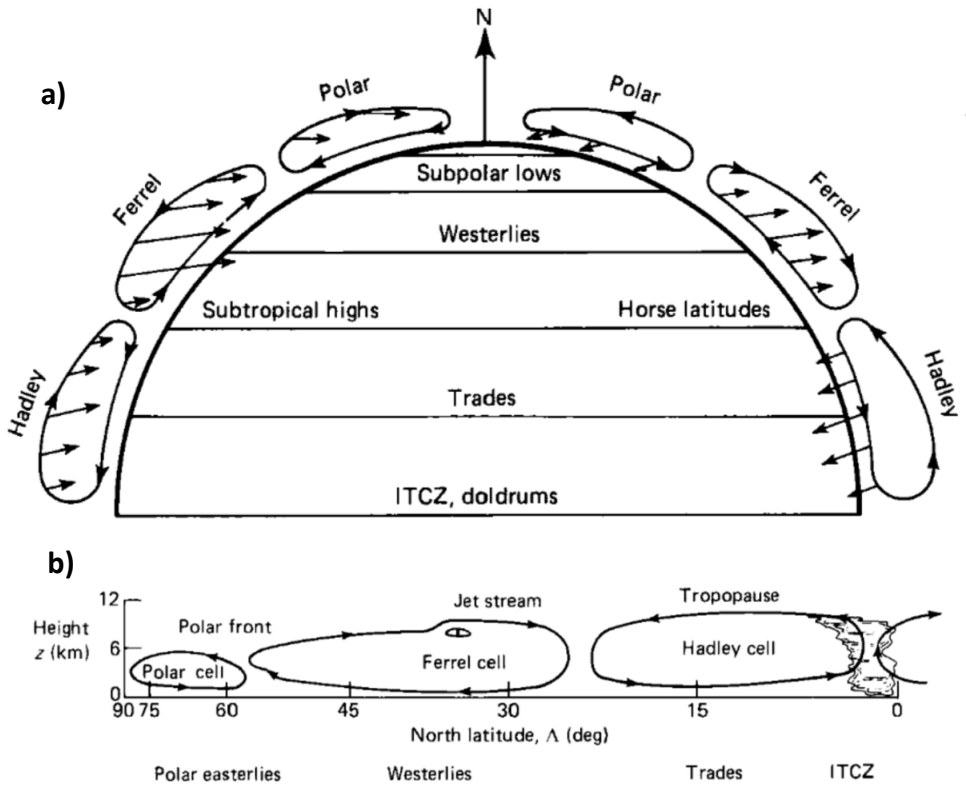


Figure 3: Reproduced from Apel (1987; Figure 2.10 (part a) & Figure 2.11 (part b)). (a) Diagram of the Northern Hemisphere large scale atmospheric circulation cells within the troposphere, showing the tropical Hadley cells, midlatitude Ferrel cells, and high latitude polar cells. (b) Vertical cross section of the three-cell circulation pattern from equator to pole, showing the elevation of the tropopause in the tropics relative to the polar regions.

is also within the lower stratosphere that the 'ozone layer' exists, which is what causes the heating and the reversal of the vertical temperature gradient within the stratosphere, as opposed to in the troposphere which is primarily heated from below.

2.1.2 Atmospheric Circulation

Within the atmosphere, in both the troposphere and the stratosphere, large scale patterns of circulation exist. In the troposphere, these exist in the form of 3 distinct circulation 'cells' as shown in Figure 3: the tropical Hadley cells, midlatitude Ferrel cells, and the high latitude (aptly named) polar cells. Reaching into the stratosphere, there exists upwelling from the troposphere

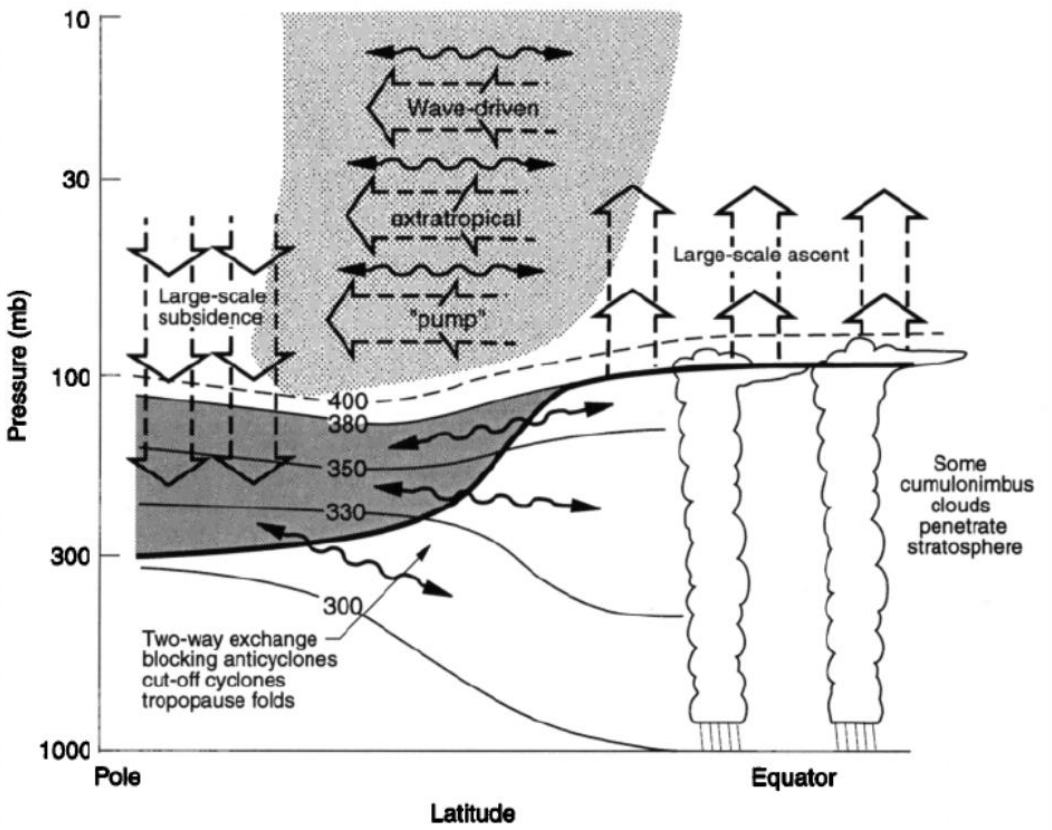


Figure 4: Reproduced from Holton et al. (1995, Figure 3). A schematic showing the dynamical aspects of stratosphere-troposphere exchange and the global Brewer-Dobson circulation. The tropopause is marked by the thick black line.

over the equator. This air is then transported polewards from equatorial latitudes towards higher latitudes, where the stratospheric airs are mixed into the troposphere via synoptic scale waves. This circulation is known as the Brewer-Dobson circulation, named in recognition of its discovery by Brewer (1949) and Dobson (1956), and is shown in Figure 4. This circulation is a wave-driven circulation, driven by upward propagating planetary scale Rossby waves from the troposphere, which dissipate (or break) and cause the poleward flow of the air in the stratosphere in order to conserve angular momentum (Butchart, 2014).

It is through this Brewer-Dobson circulation that transport occurs within the stratosphere and also how the stratosphere can influence the troposphere, and vice versa. It is also this circulation that allows gases emitted by large explosive volcanic eruptions located in equatorial latitudes to be lofted into the stratosphere and transported on the global scale, thus influencing both the

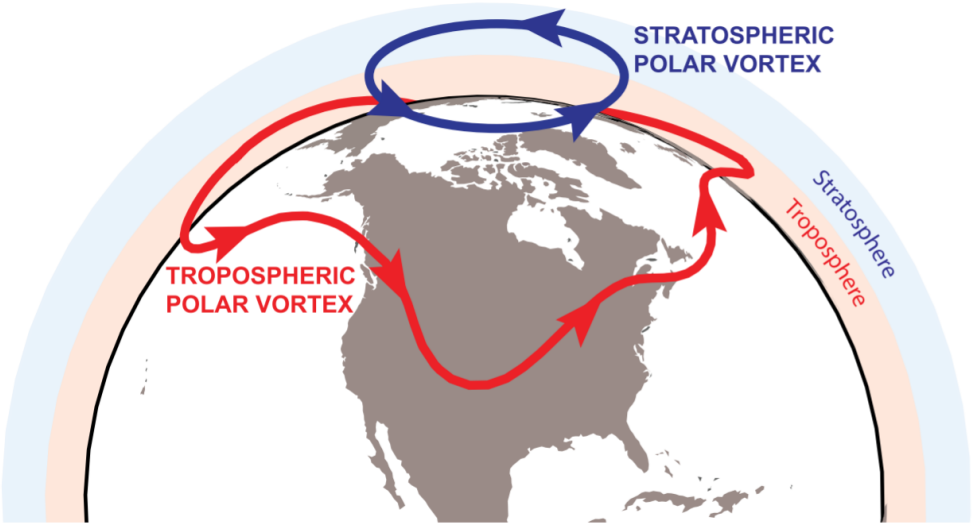


Figure 5: Reproduced from Waugh et al. (2017, figure 1). A schematic showing the stratospheric polar vortex along with the mid-latitude tropospheric jet (or tropospheric polar vortex) during the northern hemisphere wintertime.

stratosphere, and the troposphere and surface, up to a global scale. This will be discussed further in this section.

One final feature of the atmospheric circulation which is relevant to the impact of volcanic eruptions is the polar vortex. The polar vortex is a strong westerly jet of air within the stratosphere in winter which circles the pole at around a latitude of 60 degrees North/South. This jet is caused by the equator-pole temperature gradient set up within the stratosphere due to heating in the tropics from ozone absorption and the cooling of the winter polar region. During summer, this temperature gradient between the pole and the equator is reversed, leading instead to easterly winds dominating in this region of the stratosphere (Waugh and Polvani, 2010). During the winter months, the polar vortex essentially acts to keep very cold air contained at the pole, so the strength and positioning of this jet, whether it shifts or splits or weakens, has a significant impact on surface weather. Below the stratospheric polar vortex there exists another strong westerly jet, this time in the troposphere, known as the mid-latitude tropospheric jet. These two vortices/jets are illustrated in Figure 5. Volcanic eruptions have been seen to have a possible influence on this wintertime polar vortex, actually strengthening the

polar vortex (e.g. Robock, 2000), which can then potentially also affect the tropospheric jet stream (e.g. Baldwin and Dunkerton, 1999) the details of which will also be discussed further in this section.

2.2 Volcanic Eruptions

Volcanoes emit both solid matter and gases when they erupt, which have differing impacts on the weather and climate. The heavier solid particles fall out of the atmosphere relatively quickly and so do not have long-term impacts on the climate. If they reach the troposphere, they may have a lifetime of up to a few weeks, although they usually disperse after only a couple of days (Robock, 2000). Whilst this does not produce any long-term climate effects, there can be short-term impacts on the surface. These solid particles can block incoming solar radiation, which reduces the amplitude of the diurnal cycle in regions directly underneath the particle clouds. For example, after the 1980 eruption of Mount St Helens in Washington, USA, the surface temperature underneath the eruption cloud was decreased by around 8°C during the day and increased by the same amount at night (Robock and Mass, 1982). This effect lasted a few days. A similar reduction of the diurnal cycle was seen after the eruption of Krakatau in 1883 (Symons, 1888).

Eruptions also emit several different gases into the atmosphere, the most abundant of which are N_2, H_2O, and CO_2. Despite being the most abundant gasses emitted, these have little impact on the climate, even though H_2O and CO_2 are greenhouse gases. This is because the amount released during a single eruption is small compared to the atmospheric concentrations of these gases (Robock 2000). In addition, any water vapour emitted is quickly recycled through rainfall (Swingedouw et al., 2017). The gases that have the largest climatic impact are those containing sulphur, mainly SO_2 (Newhall and Self, 1982) and sometimes also small amounts of H_2S. These species react with OH and H_2O to produce sulphuric acid aerosols (H_2SO_4) with these reactions taking place on a timescale of weeks (Robock, 2000). When these aerosols are limited to the

troposphere, the aerosol particles can act as nuclei to form cloud droplets, meaning most of the aerosol here is precipitated out of the atmosphere. This means that any radiative effects in this case will be weak, localised, and relatively short lived (Swingedouw et al., 2017). This is usually the case for higher latitude or smaller, less explosive eruptions, where the emitted gases do not reach the stratosphere.

If an eruption occurs in equatorial latitudes, then there is a stronger chance that any emitted gases might reach the stratosphere, particularly if it is larger and more explosive. This is due to the upwelling circulation close to the equator (as previously described earlier in this section), which forms part of the Hadley cell circulation in the troposphere, and then the Brewer-Dobson circulation which allows for transport into the stratosphere. If these sulphuric gases reach the stratosphere before reacting to form aerosols, the resultant aerosol particles have a much longer lifetime. Sulphuric acid aerosols in the stratosphere have an e-folding time[1] of up to about a year and can be advected around the globe in a matter of weeks (Robock, 2000). For example, the aerosol cloud from the eruption of Krakatau in 1883 circled the globe in about 2 weeks (Symons, 1888), and the aerosol cloud resulting from the Pinatubo eruption in 1991 circled the globe in 3 weeks (Bluth et al. 1992). This aerosol loading in the stratosphere is not spatially uniform and depends on the exact location the eruption takes place. If an eruption occurs in extra-tropical latitudes, the resulting aerosol cloud is mostly confined to the hemisphere in which the eruption took place.

For these large equatorial eruptions, because of the Brewer-Dobson circulation the aerosols can be lifted up into the stratosphere here and then transported polewards into the midlatitudes in both hemispheres (see again Figure 4), leading to global radiative effects. The aerosols are then transported towards the surface and into the troposphere at higher latitudes, which is where

[1] The e-folding time referred to here is in relation to an exponential *decrease* in aerosols rather than an increase.

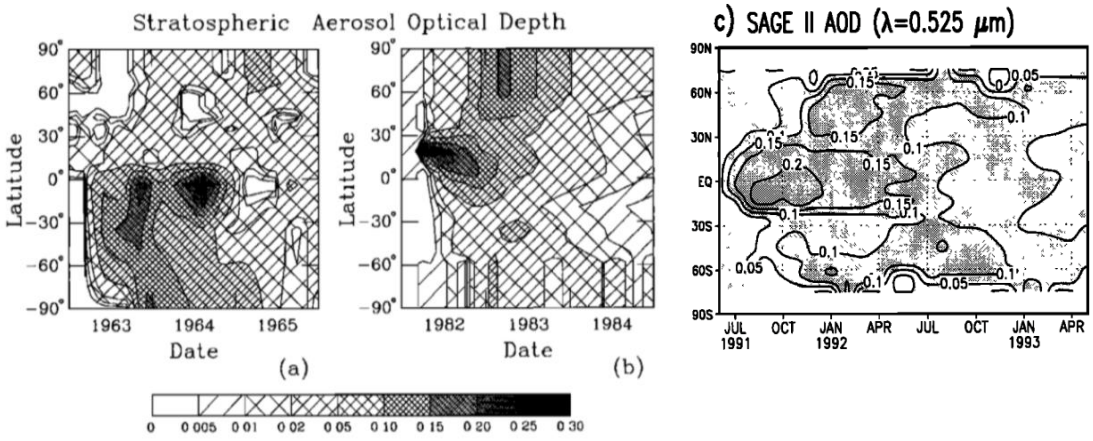


Figure 6: The estimated stratospheric aerosol optical depth at a wavelength of 0.55μm as a function of latitude and time for the years following the eruptions of (a) Agung, and (b) El Chichón, reproduced from Sato et al. (1993; Figure 2), and (c) the observed total aerosol optical depth for a wavelength of 0.525μm as a function of latitude and time for the years following the Pinatubo eruption, taken from Stenchikov et al. (1998; plot d) from Figure 3).

they are dissipated (Holton et al., 1995). This circulation takes place on a timescale of 1-2 years, which gives stratospheric aerosols their longer lifetime, and means they can produce radiative effects for up to 2 years following the initial eruption. The exact path of the aerosol cloud also depends on the background wind distribution at the time of the eruption. For example, although the locations of the 1982 El Chichón and 1991 Pinatubo eruptions are only 2 degrees of latitude apart, after one circulation of the globe their respective aerosol clouds were 25° apart, with Pinatubo's straddling the equator and extending into both hemispheres (Stowe et al., 1992) and El Chichón's remaining in the Northern Hemisphere, extending from the equator to about 30°N (Strong, 1984). The evolution of the stratospheric aerosols in terms of latitude following these two eruptions are shown in Figure 6, along with the same for the Agung eruption of 1963 (plots taken from Sato et al., 1993, and Stenchikov et al., 1998). The general locations of these resulting aerosol clouds can have an influence on the response seen at the surface. This was seen, for example, by Fujiwara et al. (2020) when looking at 11 different reanalysis datasets and analysing the volcanic response using a multiple linear regression technique. They found that the region of maximum 2m air temperature cooling following the eruption of El Chichón occurred in the Northern Hemisphere, and the corresponding peak cooling following the Agung eruption was in

the Southern Hemisphere, corresponding to the locations of the aerosol clouds shown in Figure 6.

As previously mentioned, these effects are more likely to be seen for larger eruptions at equatorial latitudes. However, if there are frequent smaller eruptions in these locations, then these aerosols may begin to accumulate and have more significant effects, and still possibly reach the stratosphere (e.g. Stocker et al., 2019). The impact of smaller more frequent eruptions, particularly those since 2000, has become more of a research interest recently, and they may have a larger impact on the climate than was originally thought and could have contributed to a general steady increase in stratospheric aerosol optical depth in the last decade (Vernier et al., 2011).

2.2.1 Radiative Effects

As previously mentioned, stratospheric H_2SO_4 aerosols produce the dominant radiative effects following a large volcanic eruption. These aerosols have a diameter about the same size as the wavelength of visible light, with an effective radius of 0.5μm and a single scatter albedo of 1 (Robock, 2000). This means that they strongly scatter solar radiation. Because of the presence of these aerosols, some incoming solar radiation is backscattered to space, which reduces the amount of solar radiation reaching the surface. This results in a net surface cooling, decreasing the global average surface temperature following an eruption. One of the first studies to note this drop in surface temperature was conducted by Lamb in 1970, and this observation has been consistently noted following recent eruptions too. For example, a drop in global average surface temperature was seen following the June 1991 eruption of Mount Pinatubo, which reached a peak cooling of 0.5K approximately 18 months after the initial eruption (Soden, 2002). However, recently Fujiwara et al. (2020) have argued that this peak cooling may have been overestimated as their analysis of reanalysis data using multiple linear regression, which takes into account the influence of other forms of climate variability, showed a peak cooling of only 0.10-0.15K.

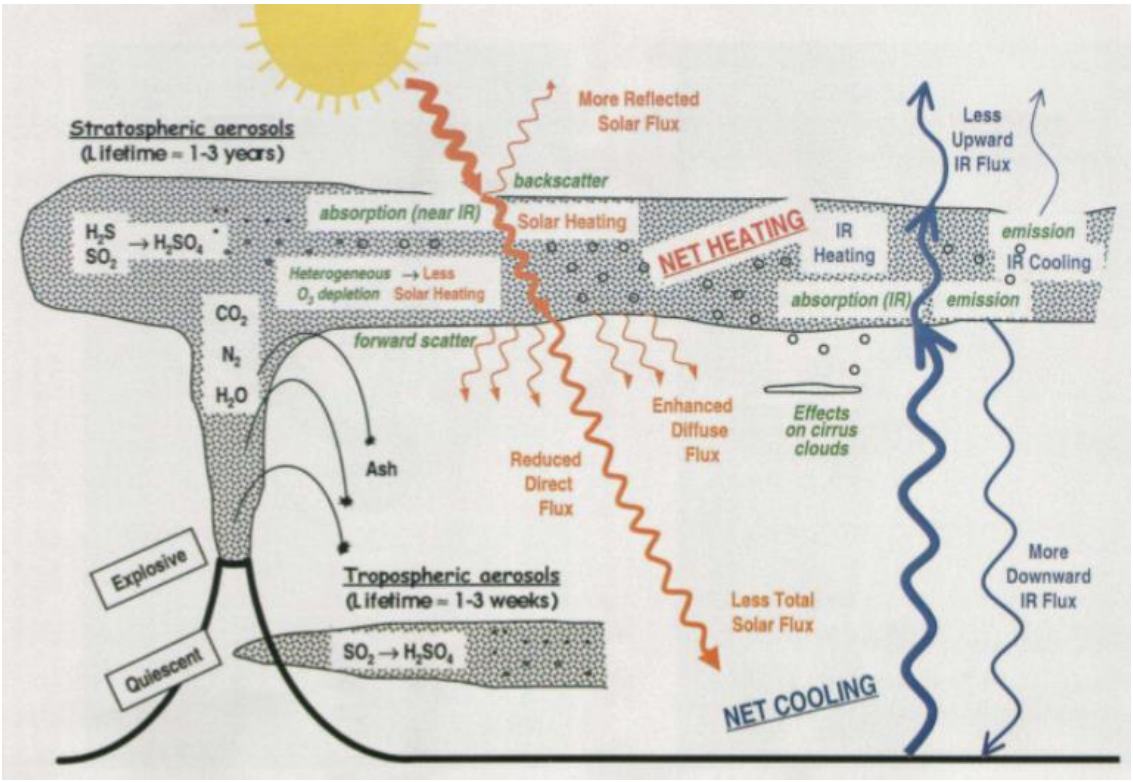


Figure 7: Reproduced from Robock (2000; Plate 1) – a schematic of the inputs into the atmosphere from a volcanic eruption and some of their effects

Swingedouw et al. (2017) also found a decrease in global average surface temperature when averaging over the months following 5 of the more recent large tropical eruptions (Krakatau, Santa Maria, Agung, El Chichón, and Pinatubo). They also found that the cooling reached a peak value between 1-2 years after the eruptions, and that it took around 5 years for the global surface temperatures to return to their 'normal' pre-eruption conditions. This surface cooling caused by stratospheric aerosols is not spatially uniform and follows the distribution of the aerosol cloud itself. This cooling effect can also be masked by El Niño events occurring shortly after or during a volcanic eruption. This has been thought to have been the case with several recent eruptions, including El Chichón in 1982 and Pinatubo in 1991 which both occurred at the same time as very large El Niño events. This has been accounted for in most studies, for example Soden (2002), who found that the cooling caused by the Pinatubo eruption reached a higher peak value if the effects of the El Niño were accounted for.

In addition to the scattering of incoming solar radiation, the stratospheric aerosols also absorb longwave near infrared (IR) radiation, which causes localised heating in the stratosphere (Robock, 2000). This warming occurs at two places within the lower stratosphere: at the top of the aerosol cloud due to the absorption of incoming solar radiation, and at the bottom of the aerosol cloud due to the absorption of upward longwave radiation from the surface and the troposphere. Mitchell et al. (2015) analysed 9 recent reanalysis datasets for 1979-2009 using regression analysis in order to separate out the signals due to different sources of climate variability and could clearly see this heating in the lower stratosphere due volcanic aerosols. They found a positive temperature anomaly in the tropical lower stratosphere in all reanalysis datasets, although the resolution of the analyses wasn't good enough to specifically separate the heating at the top and bottom of the aerosol cloud and was seen as a single area of a temperature anomaly. Figure 7 shows an illustration of some of these radiative effects (from Robock, 2000).

2.2.2 Dynamical Effects

The heating in the lower stratosphere caused by the volcanic aerosols emitted from these aforementioned large tropical eruptions is initially mostly confined to over the equator and the tropics due to the location of the resultant aerosol cloud (until the aerosols are further advected around the globe after the first year). This increases the latitudinal temperature gradient in the stratosphere between the equator and the poles. By the Thermal Wind balance equations, this enhanced North-South temperature gradient produces enhanced zonal winds in the stratosphere at mid- to polar latitudes, which strengthens the polar vortex during winter months (December-January-February; DJF). Mitchell et al. (2015) also saw this in their analysis of the reanalysis datasets, which showed a small significant westerly wind response in the Northern Hemisphere (NH) polar vortex during the winter following a volcanic eruption, extending down

into the troposphere. This polar vortex strengthening has also been found in previous studies (e.g. Robock, 2000).

This strengthened polar vortex is thought to modulate planetary waves that propagate upwards from the troposphere, causing them to break or possibly refracting them towards the equator (Kodera, 1994; Shindell et al., 2003). This mechanism stems from the criterion first proposed by Charney and Drazin (1961), which when written mathematically looks like:

$$0 < (\bar{u} - c) < u_c = \beta \left(k^2 + l^2 + \frac{f_o^2}{4N^2H^2} \right)^{-1}$$

Here, $\bar{u}$ is the mean zonal flow of the atmosphere, c is the phase speed of the wave, and u_c is called the 'Rossby critical velocity' (Holton, 1992)[2]. This criterion is derived from the quasi-geostrophic equations describing the flow within the atmosphere, where we assume a uniform background wind (with small perturbations from this mean state) and find a linear wavelike solution to these equations. When considering stationary waves in the equation above (i.e. c=0), this implies that vertically propagating Rossby waves can only propagate through a region of the atmosphere when the mean zonal flow is greater than 0 (i.e. the flow is westerly) but is less than a critical value. Otherwise, these waves get reflected or refracted. During the summer months, the mean zonal winds in the stratosphere are easterly, so no vertically propagating stationary waves can actually propagate into the stratosphere. During the winter months, the mean zonal stratospheric winds are westerly due to the temperature gradient between the pole and the equator, which produces the polar vortex. This means that some Rossby waves can propagate into the stratosphere during winter. The impact of volcanic aerosols essentially increases this temperature gradient to strengthen the polar vortex, increasing the westerly mean flow. As a

[2] The other symbols in this equation are defined as follows: β is the horizontal gradient of the Coriolis parameter, k and l are wavenumbers in the x and y directions respectively, f_o is the constant term in the linear expansion of the Coriolis parameter (in the beta-plane approximation), N represents the buoyancy of the air and H is a characteristic height scale in the atmosphere.

result, the westerly winds of the polar vortex can be too strong for vertically propagating waves to propagate through, and they are reflected back into the troposphere or refracted towards the equator. This altered planetary wave propagation, together with the fact that a strong vortex is more difficult to destroy via wave-mean flow interaction, means that the stratospheric polar vortex is relatively undisturbed by the planetary waves and thus is usually stronger than usual in a winter following an eruption. These dynamical effects in the stratosphere also influence the troposphere and surface via top-down mechanisms so that the North Atlantic Oscillation (NAO) pattern is biased towards its positive phase, and this is the surface response usually associated with the winter following a volcanic eruption. The exact mechanisms here involving the coupling between the stratosphere and the troposphere are still not fully understood however (Kidston et al., 2015).

Associated with this positive NAO phase during winter is a pattern of positive temperature anomalies over the NH continents, which is somewhat contradictory to the general global-averaged cooling observed following an eruption. This 'winter warming' pattern was first observed and linked to volcanic eruptions by Groisman (1985), who noted a warming over Russia during winters following the 10 largest eruptions since 1815. This pattern of warming was then linked to the positive NAO phase strongly observed following the eruption of Pinatubo in 1991 (Robock and Mao, 1992), and then later confirmed to be the case when considering eruptions over the entire period since 1815 (e.g. Driscoll et al., 2012). Figure 8 shows near surface temperature anomalies averaged over two post eruption winters for nine large tropical eruptions since 1870 and clearly shows this ‘winter warming’ pattern of positive temperature anomalies over the NH continents (taken from Driscoll et al., 2012).

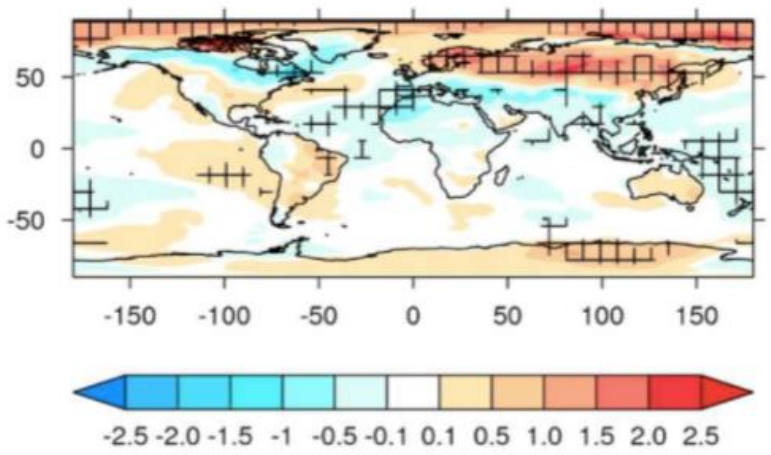


Figure 8: Taken from Figure 4 of Driscoll et al. (2012) – the composite anomaly in near surface temperature (K) using 20th Century Reanalysis data. Average is taken over the 2 post eruption winters following 9 of the largest eruptions since 1870. Hatching displays areas of over 95% significance when using a two-tailed test.

Another idea that has not been as widely explored is that a heating anomaly in the lower stratosphere can induce a dynamical response in the troposphere that causes changes in circulation in the troposphere, directly influencing the eddy processes that give rise to the midlatitude jet. This was investigated by Simpson et al. (2009) using a general circulation model (GCM) with imposed idealised temperature anomalies at different latitudes. Their study had a particular focus on the 11-year solar cycle influence, however the proposed mechanisms may also be applicable to heating in the lower stratosphere due to volcanic aerosols. Their model does not include a stratospheric polar vortex but still produces a significant response in the troposphere to stratospheric heating perturbations. The mechanisms they propose involve the heating in the lower stratosphere changing the horizontal temperature gradient, which creates a vertical wind shear anomaly that can affect smaller synoptic scale waves in the midlatitudes in the troposphere. This can then affect the tropospheric jets and therefore have an impact at the surface.

2.2.3 Impact on Ozone

Volcanic aerosols can also impact ozone in the stratosphere. In cold regions such as the tropical tropopause region, volcanic aerosols in the stratosphere can act as surfaces for the heterogeneous chemical reactions that liberate chlorine, which is active in the catalytic reactions that destroy ozone (Robock, 2000). This decrease in ozone concentration in the stratosphere causes less UV (Ultraviolet radiation) absorption, resulting in an increase in the amount of UV reaching the surface. Because the aerosols absorb and scatter various wavelengths of light, the presence of these volcanic aerosols also has an impact on the rates of the ozone reactions that involve photolysis, however this effect is small so the net effect is a decrease in stratospheric ozone due to the increase of the heterogeneous reactions described previously (Dessler, 2000).

2.2.4 Modelling the Impacts of Volcanic Eruptions

Modelling the impacts of volcanic eruptions has been the focus of many studies, however none of them seem to fully capture the dynamical effects of these large eruptions and the propagation of these effects in the stratosphere down to the surface. Analysis of models used for the Coupled Model Intercomparison Project (CMIP) from both phase 3 (CMIP3) and phase 5 (CMPI5) generally found that the positive NAO phase, strengthened polar vortex, and the 'winter warming' patterns were not well simulated (e.g. Stenchikov et al., 2006; Driscoll et al., 2012). An example of this is shown in Figure 9 (taken from Driscoll et al., 2012) comparing the composite anomaly in sea level pressure for the first two winters following nine major eruptions from reanalysis data and the multi-model mean for the CMIP5 models used. This shows clear differences between the models and the reanalysis data, with the models here barely being able to reproduce the positive NAO-like anomaly pattern seen in the reanalysis data.

Several possible reasons for this have been proposed. One idea is that you need a well resolved stratosphere in the models to get the full dynamical response (Stenchikov et al., 2006) and that

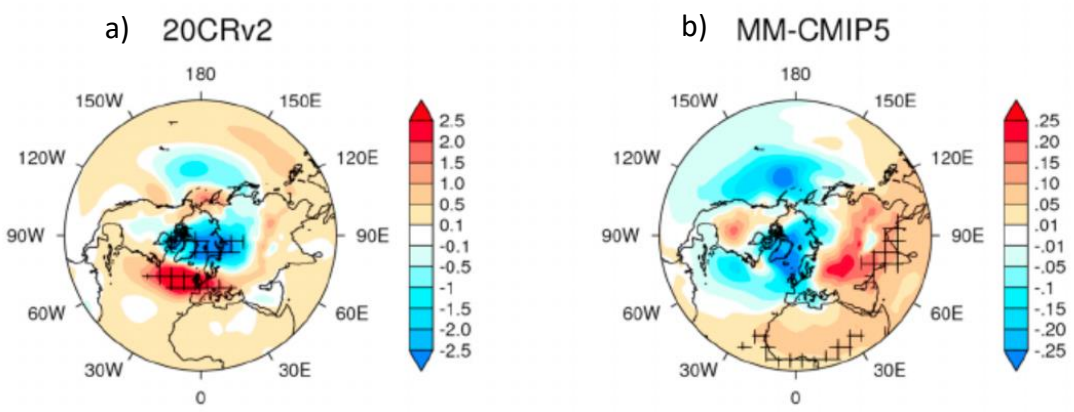


Figure 9: Taken from Figure 4 of Driscoll et al. (2012) – the composite anomaly in sea level pressure (hPa) for a) 20th Century Reanalysis data, and b) the multimodel mean of the CMIP5 models. Average is taken over the 2 post eruption winters following 9 of the largest eruptions since 1870. Hatching displays areas of a) over 95% significance when using a two-tailed test, and b) where at least 90% of the models agree on the sign of the anomaly. Note the differing scales.

the results can vary greatly depending on the quality of the volcanic eruption input data and how the model treats the evolution of the stratospheric aerosols (Timmreck, 2012). Another possible reason may be that the "volcanic aerosol" signal in the observations used to create the volcanic aerosols used in the model may contain effects other than volcanic eruptions that are wrongly attributed to the stratospheric aerosols.

Another possibility is that climate models are sensitive to the background state at the time of the eruptions. Zanchettin et al. (2013a) found that this was true, particularly when simulating the impacts on the oceans due to an eruption. However, they found that background conditions had little effect on the simulated radiative impacts. Thomas et al. (2009) found that the modelled response of the climate to an eruption was modulated by the phase of the Quasi-Biennial Oscillation (QBO). They found that simulating different QBO phases during an eruption gave different results, with differences appearing in the simulated temperature response in the lower stratosphere in the tropics and extratropics. Stenchikov et al. (2004) also investigated a model that included a realistic QBO. Using this, they found that they got more realistic temperature responses in the lower stratosphere due to eruptions, both spatially and temporally, in the experiments where the QBO was included when compared to when it was not included,

suggesting that having the correct phase of the QBO in a model is necessary to get the correct pattern of the temperature response in the lower stratosphere. They also found that, in accordance with many other studies, an easterly QBO phase produces a weaker polar vortex, and a westerly QBO phase produces a stronger polar vortex (Holton and Tan, 1982), which would potentially interfere with the dynamical response to volcanic forcing in the models.

Toohey et al. (2014) also found that the response of the polar vortex in models is sensitive to the structure and size of the volcanic forcing used and suggest that even a Pinatubo sized eruption may not be large enough to directly affect the polar vortex in the models. Another consideration is the number of ensemble members used in a modelling study when looking at volcanic impacts. Studies have found that you need a sufficiently large number of ensemble members to detect a statistically significant impact on the polar vortex due to the high internal variability of the polar stratosphere. Bittner et al. (2016) found that when considering the signal from the two largest eruptions since 1850 (Krakatau and Pinatubo) in CMIP5 models, 15 ensemble members were needed to see a significant vortex strengthening. They suggest that this minimum number of ensemble members may be model dependent.

2.2.5 Link to and Impact on ENSO

One important factor to consider when trying to isolate the impact of volcanic eruptions is the El Niño-Southern Oscillation (ENSO). Several of the more recent large tropical eruptions happened during very large El Niño years, for example El Chichón in 1982 and Pinatubo in 1991. This is indicated in Figure 1, where the eruptions are colour coded according to the ENSO phase in the first post-eruption winter. The warming associated with El Niño events can act to cancel out some of the volcanic induced cooling in both observations (Soden, 2002) and model simulations (Lehner et al., 2016), making it important to consider how to remove this effect when trying to understand the impact eruptions alone have on the climate.

Several studies have tried to see if there is a link between a volcanic eruption occurring and possibly inducing an El Niño during the following months or year, or whether the events occur by chance simply because you are likely to get an El Niño event every 2-7 years anyway. It has also been suggested that, if you look at the exact dates of the eruptions themselves, El Niño events were already in progress before the eruption began (Robock, 2000). Robock et al. (1995) attempted to test this by trying to model a mechanism proposed by Hirono (1988), which involved a breakdown of the trade winds because of heating in the lower atmosphere caused by volcanic aerosols as they fall out of the eruption cloud in the East Pacific. It was proposed that this heating would induce a low pressure region, reducing the north-east trade winds, and producing an oceanographic response to cause an El Niño. However, Robock et al. (1995) found that whilst they could model a reduction in the trade winds, it was too late and in the wrong place to induce an El Niño. Robock and Free (1995) also tested whether an eruption could produce an El Niño by looking at correlations between the Southern Oscillation Index as a measure of the ENSO phase and several different volcanic indices and ice core records. They found no significant correlations in any case. This result was also found by Self et al. (1997) when looking at large volcanic eruptions over the past 150 years.

More recently, Adams et al. (2003) used proxy ENSO reconstructions to investigate back to 1649 and found that there was roughly a doubling of the probability of an El Niño event occurring in the first winter following an eruption when looking at 13 large eruptions between 1649-1979. This result has also been found in other studies using paleo-reconstructions over the last millennium (e.g. Wilson et al., 2010), however this result may depend on which reconstruction and volcanic index you use. Emile-Geay et al. (2008) found a similar doubling in the probability of El Niño events occurring following explosive volcanic eruptions in a coupled climate model (Zebiak and Cane, 1987), but found that for this model, only eruptions larger than Pinatubo had a significant impact on the ENSO phase. The proposed mechanism here is that the volcanically induced surface cooling reduces the temperature contrast between the surface ocean and the

thermocline in the eastern equatorial Pacific, which reduces the westward climatological sea surface temperature gradient, which then weakens the trade winds. This in turn generates a feedback, further reducing the sea surface temperature gradient and resulting in El Niño-like conditions. However, this is not seen for all eruptions, particularly weaker ones.

In conclusion, several studies have looked at the possibility that volcanic radiative forcing induces El Niño events. In general, they find only strong ones (i.e. eruptions of Pinatubo size or larger) have any impact on ENSO and, rather than forcing an El Niño, they simply increase the likelihood of one developing. Nevertheless, it is still important to take into account other sources of natural variability when trying to look at the impact volcanic eruptions have on the climate as events like ENSO can mask some of the volcanic signal.

2.2.6 Long Term Impacts & the Effect of Volcanic Eruptions on the Oceans

Climate model simulations appear to show some longer-term impacts of volcanic eruptions. For example, Zanchettin et al. (2013b) found a signal showing positive NAO phases in winters following volcanic eruptions on a decadal time scale, with the associated 'winter warming' pattern (described previously) that peaks a decade after an eruption, when looking at nine strong eruptions since 1600. They called this a 'delayed winter warming' which was found in addition to the initial winter warming due to the initial positive NAO phase following an eruption. This sort of long-term response is thought to come from the impact eruptions have on the oceans since any sulphate aerosols only last up to around 2 years in the stratosphere. The mechanism proposed here is that the general surface cooling due to the volcanic eruptions can modify the ocean circulation in the Atlantic (i.e. the Atlantic Meridional Overturning Circulation (AMOC)). This can then be sustained over longer time scales due to ocean-atmosphere feedbacks, which can prolong the recovery of the climate system from the volcanic perturbations (Zanchettin et al. 2013b).

Stenchikov et al. (2009) found a reduction of ocean heat content after both the Tambora (1815) and Pinatubo (1991) eruptions in their model, as well as strengthening of the AMOC due to this cooling. The mechanism they propose also links to the impact the eruptions have on the hydrological cycle: the cooling induced by the eruption leads to reduced precipitation and river runoff at high latitudes in the NH (Trenberth and Dai, 2007), which leads to a more saline, and therefore more a dense upper ocean at these latitudes. These conditions increase oceanic convection and enhance the AMOC. The direct radiative cooling also cools the upper ocean, increasing the density and adding to this effect. They also argue that the dynamical impact of volcanic eruptions can also have an impact on the oceans and act to strengthen the AMOC. They suggest that the strengthened polar vortex acts to shift the tropospheric jet polewards increasing winds in the lower troposphere, which strengthens ocean stirring in high latitudes (Stenchikov et al., 2006). This poleward jet shift is equivalent to the enhanced positive NAO/Arctic Oscillation (AO) phases also seen (and the stronger winds over the North Atlantic associated with these, which extracts more heat from the ocean and also cools the surface) which can also lead to a strengthening of the AMOC (Delworth and Dixon, 2000).

This decrease in ocean temperature and increased salinity in the North Atlantic leading to an enhancement of the AMOC was also seen by Ding et al. (2014) in CMIP5 models following especially large eruptions (again: Krakatau, Santa Maria, Agung, El Chichón, and Pinatubo). They found that this temperature decrease reached a peak 1-2 years following an eruption, and that the response was influenced by the background state of the AMOC at the time of the eruption. They also found that this reduction in ocean heat content caused by the surface cooling effect of particularly large eruptions could persist on the decadal timescale.

However, Ottera et al. (2010) found that in their model, external forcing, like volcanic eruptions, does not account for all of the simulated internal variability in the AMOC (and the Atlantic

Multidecadal Oscillation (AMO)), instead they propose that it acts like a metronome for the Atlantic multidecadal variability.

An impact on the oceans due to volcanic eruptions has also been seen in observations and reanalysis. It has been noted that the ocean warming trend in recent decades due to anthropogenic forcing is at times offset by a cooling, which is attributed to major volcanic eruptions (Balmaseda et al., 2013). This has also been seen in model reconstructions (e.g. Stenchikov et al., 2009). Since very strong tropical eruptions have been happening fairly periodically in the past few hundred years (Tambora in 1815, followed by Krakatau in 1883 etc.), the effects in the oceans can accumulate as subsequent eruptions interrupt the relaxation time in the ocean, which is around 100 years (Stenchikov et al., 2009). Because of this, the oceans haven't fully recovered from an eruption before the next one has occurred.

2.3 Summary and Thesis Objectives

As shown in this section, there are several open questions that remain when investigating the impact of volcanic eruptions on the climate. What exactly are the underlying mechanisms that drive the surface and atmospheric responses, for example particularly those involving the stratosphere? And how can climate models better simulate the observed responses and be used to improve our understanding of the mechanisms? Furthermore, what are the mechanisms that govern potential longer-term impacts of eruptions and their impact on the oceans? In order to answer these, we also need to make sure we have an in depth understanding of exactly what those surface impacts are.

In this thesis, I aim to expand on previous work which investigated the surface response of these large tropical volcanic eruptions. I use a multiple linear regression method (described in the following section) to build on the methods used by previous studies, especially those that have used a composite average analysis such as Driscoll et al. (2012). I also investigate the winters

following an eruption separately by looking at yearly lags, and extend these to a lag of 5 years to investigate any slightly longer-term volcanic signals. I also focus on shorter periods of regression analysis centred on specific large eruptions to investigate any differing responses to certain eruptions given that this has been seen to some extent previously, particularly when considering the 1963 Agung eruption. I further extend previous work by looking at the volcanic signal in the North Atlantic jet using indices representing the speed and latitude, and also atmospheric blocking, in addition to looking at the signal in SLP, SSTs, and the NAO. The main objective of this is to compare to previous studies to further validate the main results (e.g. the positive NAO phase found in the first two post-eruption winters) and extend this by looking at these results in more detail as described above. This will provide further detail on the surface response to these volcanic eruptions and provide further questions that can be investigated by analysing more fields or using modelling studies, for example investigating the stratospheric circulation and the underlying mechanisms to gain a better understanding of these since these are both still open questions in this area of research.

3. Data & Methodology

Multiple linear regression analysis is used here to look at the volcanic response in various fields, including mean sea level pressure (SLP), sea surface temperature (SST), the NAO index, the latitude and speed of the North Atlantic jet, and blocking events. The regression method is first described, including the data used as regression indices and a discussion of other indices used to describe volcanic eruptions, followed by a description of the analysed data.

3.1 Multiple Linear Regression

Multiple linear regression is a method used to find the best fit of a linear combination of different timeseries to another particular timeseries. The basic model used here is:

$$y(t) = \sum_{i=0}^{n} \beta_i x_i(t) + \epsilon(t)$$

where $y(t)$ is the observed variable timeseries, $x_i(t)$ are the different forcing timeseries ('regression indices'), β_i are the regression coefficients associated with forcing $x_i(t)$, and $\epsilon(t)$ represents the residual, or noise term. The regression is performed for each individual latitude/longitude gridbox for fields which are not simply a single timeseries of data. The sum is taken over all the regression indices used in the analysis.

The climate forcings used as regression indices in this particular analysis include representations of variability associated with the solar cycle (both the 11-year cycle and a smoothed long-term trend), ENSO, the AMO, and volcanic eruptions. These indices are shown in Figure 10 and explained in further detail below. A linear trend is also included as an index to represent anthropogenic warming over the period of the regression. All the results presented here look at the NH wintertime responses to volcanic eruptions, i.e. the December-January-February (DJF) averaged responses, and are focused on the North Atlantic/European sector (30°W-40°E; 30°N-70°N).

Many studies have used this technique to look at the signals coming from various sources of climate variability, including the 11-year solar cycle (e.g. Gray et al., 2016 & 2013; Crooks and Gray, 2005), as well as ENSO, the QBO, and volcanic eruptions (e.g. Mitchell et al., 2015; Fujiwara et al., 2015).

A lagged response to volcanic eruptions is also investigated using the regression analysis. This is done by lagging the volcanic timeseries a number of years behind all the other timeseries used in the regression (with all the other indices held at a 0 lag) to show the winter responses in the years following the eruptions. This means that the 'lag 0' response is equivalent to the 1st winter response following the eruptions, and 'lag 1' corresponds to the 2nd winter, and so on. This is

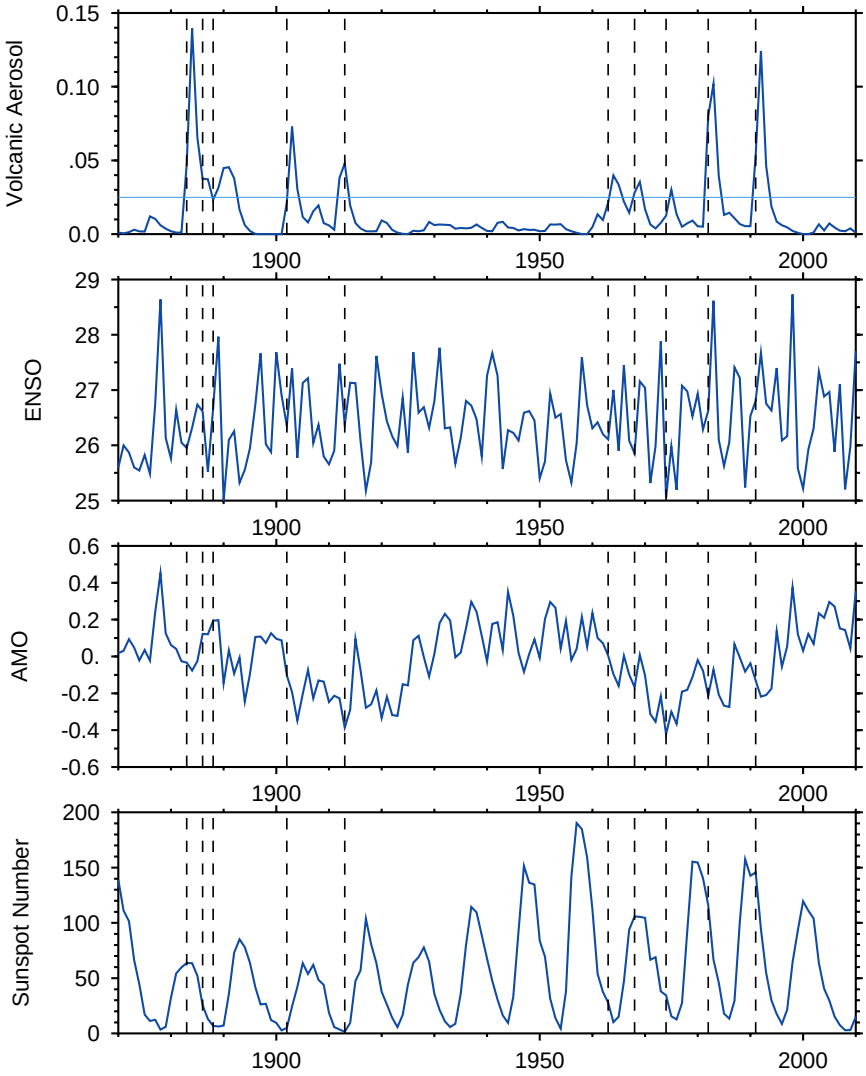


Figure 10: Timeseries of the main regression indices used in the regression analysis, representing variability associated with volcanic aerosol (stratospheric aerosol optical depth), the El Niño-Southern Oscillation (ENSO; °C), the Atlantic Multidecadal Oscillation (AMO; °C) and sunspot number, as used in Gray et al. (2016). The horizontal line on the volcanic aerosol timeseries indicates an aerosol optical depth value of 0.025. The dashed vertical lines on all plots show the dates of the 10 eruptions with aerosol peaks higher than this value (see Table 1 for more details).

done to consider how the volcanic signal evolves following an eruption. It also allows comparison to previous composite studies, which tend to average the responses in the 1st and 2nd winters following a volcanic eruption (e.g. Driscoll et al., 2012) and to see whether this is a good method. When including the lagged response, the model becomes:

$$y(t) = \sum_{i=0}^{n-1} \beta_i x_i(t) + \beta_{VOLC} x_{VOLC}(t-l) + \epsilon(t)$$

where l is the value of the lag in years, ranging from 0 to 5 in this case.

A physical consideration to try to take into account when doing this type of analysis on the climate system is the fact that atmospheric data tends to have an element of autocorrelation. This means that each data point in the timeseries used for a given forcing depends to some extent on previous data points in the same timeseries. Using an autoregressive noise model in the regression analysis attempts to account for this autocorrelation. An AR(1) (order 1) model is used here, largely to be consistent with more recent studies which have used a similar regression method (Gray et al., 2016 & 2013, Mitchell et al., 2015). This allows for a relationship between a data point and a previous data point one time step apart. Previous studies have shown that this method of regression analysis is largely insensitive to the order of the autoregressive noise model used. When this method was originally used by Crooks and Gray (2005), an autoregressive model of order 3 was used, but they commented that the patterns shown in their results appeared to be insensitive to whether an order 1, 2, or 3 model was used. Gray et al. (2013) made a similar comment after performing sensitivity tests on the various orders of autoregressive models and decided to use a model of order 1. An AR(1) model was also used by Mitchell et al. (2015) when also looking at the volcanic response in regression analysis of reanalysis datasets, most of which were of a much shorter time period than the datasets used here. Crooks and Gray (2005) noted that because their regression analysis included a QBO component, they decided to use a model of order 3 to account for any periodicity in the residual term greater that one time step which might have been coming from this QBO term. However, a QBO index is not included in the regression model used here as data for this was not available for time periods prior to 1953. Also following the previous studies mentioned, a two-sided Student's t-test was used to determine the probability that the regression coefficients differed significantly from noise.

The timeseries used in the regression analysis are all deseasonalised, removing their annual cycles to produce a timeseries of anomalies. They are then normalised by dividing by their standard deviation, so they are expressed in terms of standard deviations from their mean value. The desired response, in this case volcanic, is then rescaled following the regression analysis, multiplying by the difference between the maximum and minimum values of the timeseries divided by the standard deviation of the timeseries, i.e. $\frac{\max(x_{VOLC})-\min(x_{VOLC})}{\sigma(x_{VOLC})}$. In this case, the results then provide an estimate of the maximum likely response due to the largest eruption during the time period of the regression analysis.

A drawback of using this technique is that it assumes that all the timeseries used in the regression analysis are linearly independent of each other. This is not the case for a system like the atmosphere where there are nonlinear interactions between different sources of variability. However, it is still a method used in these circumstances as it attempts to separate out the influences of the different climate forcings, represented by the timeseries, which is useful when wanting to focus on the influence of one particular forcing, such as solar or volcanic. Previous volcanic studies that only use a composite analysis risk the results of the composites being influenced by these other forcings, e.g. ENSO as discussed before, unless their influence is removed before the composite is taken.

Another thing to try to account for when using this method of analysis is any possible aliasing between the different regression indices. This is particularly important for the volcanic index since the two large peaks corresponding to the eruptions of El Chichón and Pinatubo both occur during times of solar maximum (in the 11-year cycle) and El Niño phases of ENSO, leading to potential aliasing between the volcanic index and the 11-year solar cycle and/or the ENSO indices (e.g. Chiodo et al., 2014). However, in line with other studies, sensitivity tests were performed when doing the regression analysis here to try to test for possible aliasing. These tests consisted of performing the regression analysis and removing different combinations of

the regression indices (for example, removing the ENSO index or the 11-year solar index) to test whether this had any obviously significant effects on the results. In the case of the volcanic index analysed here, the exclusion of these indices had no significant effect on the volcanic response, suggesting that the regression isn't attributing too much of the volcanic signal to the solar or ENSO signals due to aliasing.

3.2 Volcanic Indices

Some of the first indices used to describe volcanic eruptions were Lamb's Dust Veil Index (DVI; Lamb, 1970) and Mitchell's index (Mitchell, 1970). However, these indices were often derived based on climatic information so are in fact not very useful when wanting to look at the specific impacts of eruptions.

One of the more commonly used measurements of the strength of a volcanic eruption is the Volcanic Explosivity Index (VEI; Newhall and Self, 1982). This is based on an estimation of how explosive an eruption is and takes into account the amount of tephra ejected. It uses a logarithmic scale with values from 0-8, with 8 being the most explosive. The VEI values for 10 of the largest eruptions since 1870 are shown in Table 1. This sort of index is not very useful when wanting to investigate the dynamical effects of an eruption, however, as it has no information about the amount of gases ejected during an eruption or the height the gases reach in the atmosphere.

To get a longer historical dataset, information about the amount of sulphur ejected during an eruption can be obtained by looking at ice cores. The amount of sulphate aerosol deposited in these ice cores can be used to infer the amount that was present in the atmosphere following an eruption. This information gives a better indication of how the optical depth in the atmosphere is changed and the direct radiative impacts of an eruption. An example of an index that utilises ice core data is the Ice Core Volcanic Index (IVI; Gao et al., 2008), which is a volcanic

aerosol timeseries for the past 1500 years. This dataset was created using many ice cores from multiple sites, which reduces the overall errors in the data. However, large uncertainties still remain when using ice core data. For example, Gao et al. (2008) found that for the 1815 Tambora eruption deposits there was a spatial variation of around 50% among both Arctic and Antarctic ice cores, which could be even higher for smaller eruptions. They also found that when trying to consider the season of the eruptions or different criteria used to identify an eruption, each of these introduced up to an additional 10% uncertainty in the forcing dataset.

For the shorter time period used here (1870-2010), an updated annually averaged timeseries of global stratospheric aerosol optical depth is used as the volcanic regression index, taken from Sato et al. (1993). This index is expressed as the optical depth at a wavelength of 0.55μm. It is derived using information from Mitchell (1970) about the amount of material ejected during eruptions from 1850-1882, then using optical extinction data from 1882, and then satellite data from 1979 to the present day. This data is more accurate than the VEI or IVI for the most recent period as it is based on direct observations of the volcanic aerosol in the atmosphere. The timeseries used here is globally averaged. For the time period prior to satellite observations, in order to derive this timeseries assumptions were made as to the spatial distribution of the aerosols following an eruption due to the lack of observational data at multiple locations, for example that the aerosols were uniformly distributed over the globe during the 1850-1882 period and that the distribution of aerosols for the following period (1883-1959) were related to the locations of the eruptions and inferred from observations made more in the northern hemisphere. Observations were made in both hemispheres for 1960-1978, however some interpolation was still required as observations were still only made in limited latitude bands. Full details of the assumptions can be found in Sato et al. (1993). From 1979 onwards, the aerosol optical depth timeseries was derived from extensive satellite observations of both hemispheres at all latitudes, with some gaps filled by non-satellite observations. To look in more detail at the effect of volcanic eruptions where the emitted aerosols are confined mostly to one

hemisphere, such as the 1963 Agung eruption, a hemispheric mean aerosol optical depth timeseries could be used (for example, also from Sato et al., 1993 – see their Figure 1). However, due to the limited observations in the southern hemisphere during certain periods of time for example, these individual hemispheric averaged timeseries may not be completely accurate.

3.3 Other regression indices

ENSO variability for this period (1870-2010) is represented using monthly averaged sea surface temperatures taken from the Hadley Centre Sea Ice and Sea Surface Temperature (HadISST) dataset (www.metoffice.gov.uk/hadobs) averaged over the "Niño 3.4" region (5°S-5°N; 170-120°W). The solar variability is represented using the annually averaged sunspot number, which is interpolated to provide the seasonally averaged values in order to focus on the wintertime responses. As in previous regression studies (Gray et al., 2013 & 2016), the Wolf sunspot number is used, which is available back to 1700 (WDC-SILO, Royal Observatory of Belgium, Brussels; http://sidc.oma.be/silso/datafiles). This timeseries represents the 11-year solar cycle variation, and is smoothed using an 11- year filter to give a second timeseries representing the long-term solar trend. The AMO index is taken from the National Oceanic and Atmospheric Administration (NOAA; http://www.esrl.noaa.gov/psd/data/timeseries/AMO: Enfield et al., 2001) and is available for the region 0-75°N and 10°E-75°W from 1856. A linear trend is also included in the regression, as mentioned previously.

A QBO index was not used for this time period, as this index is derived from radiosonde observations of equatorial winds, which are only available from 1953. However, when the index was included in the regression analysis for the time periods which are after this time (e.g. the regression for 1980-2010), there was little change to the results, so only the results without the QBO index are included here. Figure 10 shows the main regression index timeseries used in this analysis.

3.4 Volcanic Eruptions & Regression Periods

The top plot of Figure 10 shows the timeseries used to represent volcanic eruptions in the regression, which is a timeseries of annually averaged stratospheric aerosol optical depth. The horizontal line marks an aerosol optical depth value of 0.025, and the vertical dashed lines show the eruption dates of tropical volcanoes whose eruptions resulted in an aerosol optical depth value above this line. This gave ten eruptions, further details of which are shown in Table 1.

This table shows the dates and locations of these 10 eruptions, as well as some other climate parameters at the time of, or in the first winter following, the eruptions, to get an idea of the background conditions at the time of the eruptions. These include the 1st winter NAO and East Atlantic pattern (EA) indices, the QBO phase, the 1st winter ENSO phase, the AMO phase, and the point in the 11-year solar cycle at the time of the eruption. The table also shows whether a sudden stratospheric warming (SSW) occurred in the first winter following the eruptions, according to the list of SSW events in Mitchell et al. (2013), to get an idea of how stable the polar vortex was in these winters.

The convention for defining the '1st winter' following an eruption follows that used in Driscoll et al. (2012), meaning that for eruptions happening late in the year the '1st winter' used is actually the 2nd winter DJF period after the date of the eruption. This affects the Santa Maria and Fuego eruptions, both of which erupted in the October of their eruption years. Figure 1 (Section 2) shows the locations of these eruptions on a map, along with the VEI value and ENSO phase, as well as more strong eruptions since the 19th century.

These eruptions were chosen in order to give a similar sized sample of eruptions to those used in previous studies. For example, the eruptions listed here differ only slightly to those used by Driscoll et al. (2012), with the addition of Colima (1913) and Fernandina (1968), and the exclusion of Quizapu (1932) since there is not a large peak in the stratospheric aerosol optical

Eruption	Date	Location	VEI	1st winter DJF NAO index	1st winter DJF EA index	QBO phase	1st winter ENSO phase	Point in solar cycle	AMO	SSW in first winter?
Krakatau	27 Aug 1883	Indonesia	6	1.81	-	-	neutral	max	neutral	-
Tarawera	10 Jun 1886	North Island, New Zealand	5	1.20	-	-	La Nina	mid descending	positive	-
Bandai	15 Jul 1888	Japan	4	0.15	-	-	El Nino	min	positive	-
Santa Maria	24 Oct 1902	Guatemala	6	1.44	-	-	La Nina	min	neutral	-
Colima	20 Jan 1913	Mexico	5	1.30	-	-	El Nino	Min	negative	-
Agung	17 Mar 1963	Indonesia	4	0.14	-0.44	W	El Nino	min	neutral	No
Fernandina	June 1968	Galapagos Islands, Ecuador	4	-1.81	-0.79	E	El Nino	max	negative	No
Fuego	10 Oct 1974	Guatemala	4	0.7	-2.25	E	La Nina	min	negative	No
El Chichon	4 April 1982	Mexico	5	1.14	-0.6	W	El Nino	max	negative	Yes
Pinatubo	15 Jun 1991	Philippines	6	1.39	-0.68	E	El Nino	max	negative	Yes

Table 1: Details for the 10 volcanoes with peaks in the volcanic aerosol timeseries above a value of 0.025 (see Figure 10). The VEI values (Newhall and Self, 1982) are taken from Simpkin and Siebert (1994) and the Smithsonian Institution (www.volcano.si.edu). The NAO index is taken from https://crudata.uea.ac.uk/cru/data/nao/ as described in Section 3.5. The EA index is taken from ftp://ftp.cpc.ncep.noaa.gov/wd52dg/data/indices/ea_index.tim . The ENSO phase was taken from Fig. 1 of Wunderlich and Mitchell (2017). Details about the occurrence of a sudden stratospheric warming (SSW) are taken from Mitchell et al. (2013). The other details are taken from the regression indices used here in the regression analysis. The defined '1st winter' for eruptions late in the year (Santa Maria and Fuego) is taken as the 2nd winter (DJF) following the eruptions, following Driscoll et al. (2012).

depth data following this eruption. This also includes more eruptions than quite a few studies which only average the effects of the 5 largest eruptions during this time period, for example Swingedouw et al. (2017) who look at the eruptions of Krakatau, Santa Maria, Agung, El Chichón, and Pinatubo. These ten eruptions served as a guide when deciding on smaller time periods to analyse with a view to investigating whether different eruptions had different effects on the climate. These time periods were chosen to be centred as well as possible on the large tropical eruptions, whilst keeping them as separated as possible. However, time periods that only included one very large eruption were not possible due to several eruptions happening in quick succession, for example El Chichón occurring 8 years after Fuego and 9 years before Pinatubo. This would have led to regression periods of only around 10 years, which is not really long enough to produce robust results. Because of this, some eruptions were grouped together based on which ones seemed to have similar impacts. This gave the following shorter time periods encompassing the following eruptions:

- 1870-1900: Krakatau (1883), Tarawera (1886), and Bandai (1888)
- 1895-1925: Santa Maria (1902) and Colima (1913)
- 1950-1980: Agung (1963), Fernandina (1968), and Fuego (1974)
- 1980-2010: El Chichón (1982) and Pinatubo (1991)

These shorter time periods were analysed in addition to the entire data period from 1900-2010 (or 1870-2010 in some cases).

3.5 Analysed Data

3.5.1 Observational Data

Observational datasets for SLP and SSTs were analysed using the regression analysis and the volcanic response was focused on for the North Atlantic region.

Plots showing the global DJF response from the regression analysis at a zero-year lag are shown in Figure 11 for SLP and Figure 12 for SST for several indices used in the regression, namely ENSO, the AMO, the Solar Cycle, and volcanic eruptions. These are consistent with what you might expect to see and what has been seen in previous studies. For example, the global SST response to volcanic forcing shown in Figure 12 is generally a cooling, particularly centred on the equatorial latitudes, with the tripole pattern you would expect from a positive NAO phase appearing over the North Atlantic (e.g. Hurrell et al., 2003), along with a corresponding positive NAO-like pattern appearing in the SLP response in Figure 11. This positive NAO phase is what has been seen in the first winter following an eruption, as described in Section 2.2. In addition, you can clearly see the ENSO response in SST with the expected warm tongue-like pattern in the pacific, again with the corresponding SLP anomalies present in Figure 12. The response shown

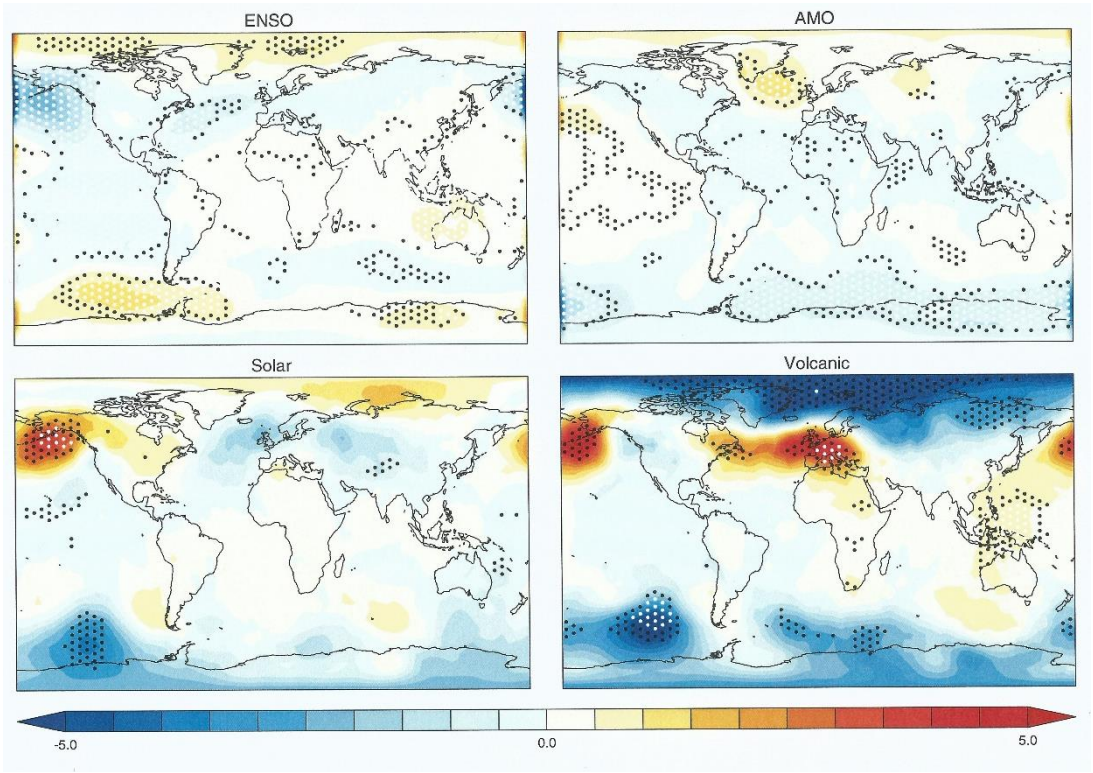


Figure 11: DJF-averaged response (hPa) from the regression analysis of mean sea level pressure (SLP) from the HadSLP observational dataset at lag 0, showing the global response associated with variability in a) ENSO, b) the AMO, c) the Solar Cycle, and d) Volcanic eruptions for the period 1870-2010. The regression coefficients have been scaled to show the maximum likely response during the time period, (e.g. for volcanic, the maximum likely response to the largest eruption within the time period). Black and white stippling shows regions of 95% and 99% significance respectively.

in the solar cycle results are also highly consistent with what you would expect from previous results (e.g. Gray et al., 2013), further confirming the results of this method.

It is worth noting the scaling in Figures 11 and 12; the figures are scaled to show the maximum likely response in SLP (fig. 11) or SST (fig. 12) during the time period, which is based on the variability of the specific index focused on. For example, for the volcanic index this would be the maximum likely response to the largest eruption within the time period, which would be the eruption of Krakatau in this case, and for the solar signal this would be the maximum likely response for the difference between solar maximum and solar minimum. As the different indices have different amounts of variability (as shown in Figure 10), due to the scaling used, comparing the magnitude of the scaled signals is not really possible. The plots here demonstrate the overall spatial patterns of variability associated with ENSO, the AMO, the solar cycle, and volcanic eruptions.

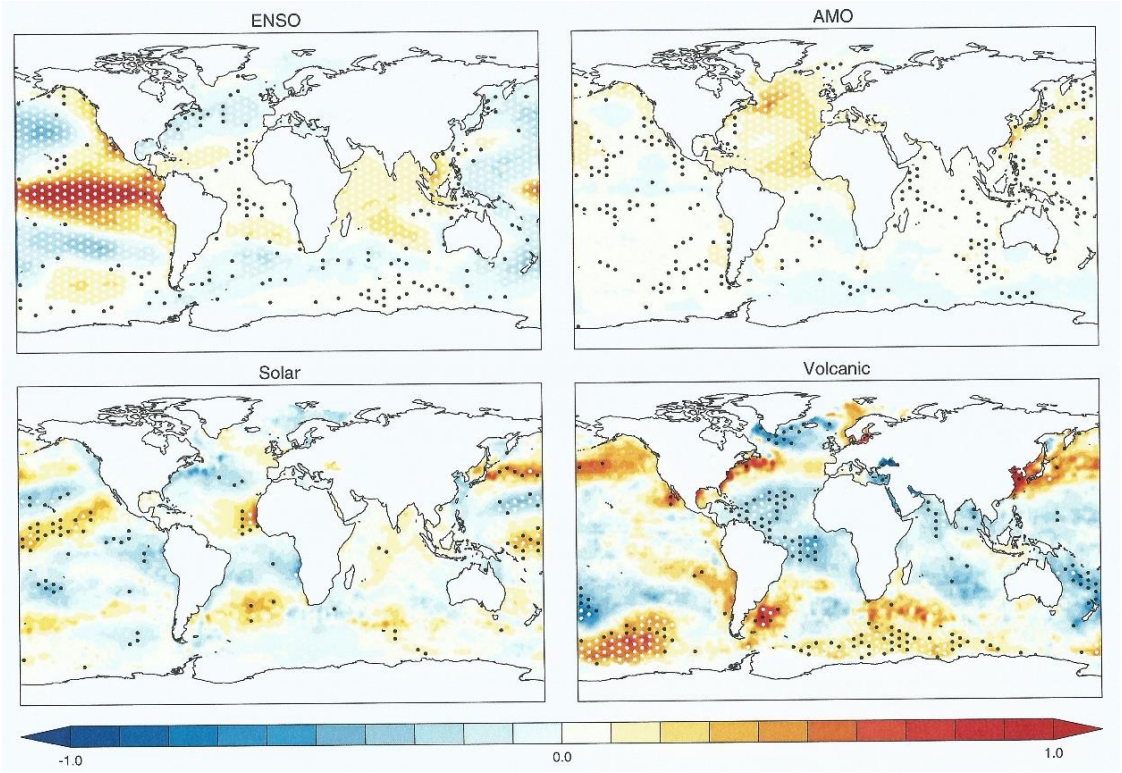


Figure 12: As Figure 11, but showing the response (K) from the regression analysis of sea surface temperature (SST) from the HadISST observational dataset.

The observational datasets used are described in more detail below:

a) Sea Level Pressure

Data for the monthly averaged gridded mean sea level pressure (SLP) is taken from the global Hadley Centre Sea Level Pressure (HadSLP2) dataset (Allan and Ansell, 2006) for the period 1870-2004 and extended to 2010 using the HadSLP2r dataset (http://www.metoffice.gov.uk/hadobs). These datasets are purely based on observations rather than using reanalysis techniques.

b) Sea Surface Temperatures

Data for the sea surface temperature (SST) analysis is taken from the Hadley Centre HadISST dataset for 1870–2010 (Rayner et al., 2003; www.metoffice.gov.uk./hadobs). This is also a purely observational dataset.

c) NAO

The NAO index used here is an updated timeseries calculated from the difference between the normalised SLP over Gibraltar and the normalised SLP over Southwest Iceland (Jones et al., 1997; https://crudata.uea.ac.uk/cru/data/nao/). This is slightly different to the traditional sites used to calculate the pressure differences, with the southern site usually taken over the Azores,

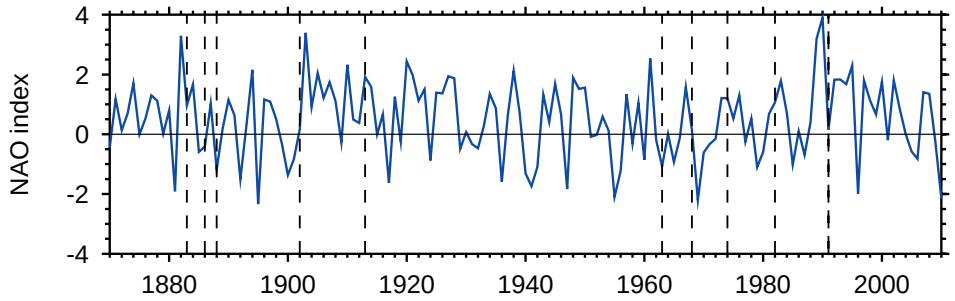


Figure 13: Timeseries for the NAO index analysed in the regression analysis. The NAO index is taken from https://crudata.uea.ac.uk/cru/data/nao/ and described in Section 3.2. The dashed vertical lines show the dates of the 10 eruptions listed in Table 1.

however using this different southern site allows the index to be extended back to 1823. Figure 13 shows the DJF averaged timeseries of this NAO index.

3.5.2 Reanalysis Data

In addition to the observational data analysed in order to investigate the volcanic response in mean SLP and SST, several different reanalysis datasets are also analysed. This is done first as a comparison to the observational data, and then to investigate the volcanic response in the North Atlantic jet, using the 850hPa zonal wind (850hPa u) and blocking events, using the 500hPa geopotential height (z500). Details of how the indices representing these fields were calculated are presented later in this section.

The reanalyses used in the regression analysis include:

- ERA-20C - a reanalysis produced by the European Centre for Medium-range Weather Forecasting (ECMWF; Poli et al., 2016)
- 20CR - Twentieth Century Reanalysis produced by the National Oceanic and Atmospheric Administration (NOAA; Compo et al., 2011)
- NCEP-NCAR - a reanalysis produced by NOAA's National Centres for Environmental Prediction (NCEP) and the National Centre for Atmospheric Research (NCAR; Kalnay et al., 1996)

Some further details of these reanalyses are found in Table 2, including a summary of which fields have been used from each reanalysis.

Reanalysis datasets differ from observational datasets in that they combine observations with a numerical model of the atmosphere to try to 'fill in the gaps' in the observations, giving a 'best guess' of the atmospheric state at a given time. The observations are used to try to constrain the model to keep it aligned with reality as closely as possible. Different reanalyses use different

Reanalysis System	Forecast model	Horizontal grid spacing	Vertical levels	Top level	Lower boundary conditions data sets	Data set reference	Data Assimilation Method	Period available	Fields analysed
ERA-20C	IFS Cycle 38r1 (2012)	N80 (TL159): ~ 125 km	91	0.01 hPa	*SSTs:* HadISSTv2.1.0.0	Titchner and Rayner (2014)	4D-Var	1900 - 2010	SLP SST 850hPa u
20CR	NCEP GFS (2008)	F47 (T62): 1.875◦	28	~2.511 hPa	*SSTs:* HadISST1.1	Rayner et al. (2003)	EnKF - 56 ensemble members	1851 - 2014	SLP 850hPa u
NCEP-NCAR	NCEP MRF (1995)	F47 (T62): 1.875◦	28	3 hPa	*SSTs:* Met Office GISST (Jan 1948 – Oct 1981) NOAA OISSTv1 (Nov 1981 – Dec 1994) NOAA OISSTv1 (Jan 1995 – present) *Sea ice:* Navy/NOAA JIC (Jan 1948 – Oct 1978) SMMR and SSM/I (Nov 1978 – present)	Parker et al. (1995) Reynolds and Smith (1994) Reynolds and Smith (1994) Kniskern (1991) Grumbine (1996)	Frozen analysis/forecast system	1948 - 2010	Z500

Table 2: Basic specifications of the reanalysis forecast models and sources of SST and sea ice lower boundary conditions used in reanalyses. Taken from Table 2, Table 4, and main text of Fujiwara et. al (2017). Also, time periods available from the reanalyses and a list of the fields analysed in the regression analysis.

models, different observational datasets to constrain their models, as well as different methods to merge the observational data they are using with the model (a process which is called data assimilation). This naturally leads to differences between different reanalyses. A further issue is the lack of observational data in certain areas of the atmosphere, particularly the upper stratosphere, which can lead to further discrepancies with the reanalysis data. These are all things to bear in mind when analysing these datasets, as noted in Fujiwara et al. (2017).

The reanalysis datasets chosen for use here were selected largely to be consistent with previous studies which did similar analysis, for example Woollings et al. (2015) for the jet and Gray et al. (2016) for the blocking. The ERA-20C dataset was chosen to add another comparison, and because of its relatively long time period of data dating back to 1900 which is more desirable when looking at volcanic impacts due to the sporadic nature of eruptions. It is also worth considering the reliability of the data for these reanalyses particularly within the stratosphere. For example, Gerber & Martineau (2018) found that the Northern Annular Mode (NAM) in the stratosphere when calculated using the 20CR dataset differed from that obtained from more modern reanalysis products, which may raise questions about the stratospheric origin of the surface and tropospheric signals presented here when using this data. However, in this instance I am using these datasets to examine the surface impacts and in order to be able to use reasonably long datasets. To look into the stratospheric response in more detail, you would want to use a reanalysis product that is more reliable within the stratosphere and so would want to focus on a shorter, more recent time period, for example using ERA-Interim which is available from 1979.

Further details of the specific fields used in the regression analysis are given below, along with a description of how the jet and blocking indices were calculated.

a) SLP & SSTs

The volcanic response in mean SLP is also analysed for the ERA-20C and 20CR reanalyses, and the response in SSTs is analysed in the ERA-20C reanalysis, both as a comparison to the observations.

b) North Atlantic Jet

The indices for jet latitude and jet speed are derived using the 850hPa zonal wind taken from the 20CR dataset for the period February 1871 – January 2008 (giving full DJF winter periods for 1872-2007 with the year labelled by the January). The indices are calculated following the method used in Woollings et al. (2015 & 2014). The algorithm for deriving the jet latitude and speed, originally used in Woollings et al. (2010a), is as follows:

- The daily mean zonal wind at 850hPa is zonally averaged over the North Atlantic (0-60°W), neglecting any winds equator ward of 15°N or poleward of 75°N
- This zonally averaged field is passed through a 10-day low pass filter, which acts to remove some short timescale noise
- The maximum westerly wind speed for each day in the resulting profile is identified and this is defined as the jet speed. The latitude at which this maximum speed is found is defined as the jet latitude.
- These daily values are averaged over each DJF winter season to give the winter average values.

The 20CR data gives 56 ensemble members, which are averaged over to create single jet latitude and jet speed timeseries. Figure 14 shows the timeseries of the DJF averaged jet latitude and speed.

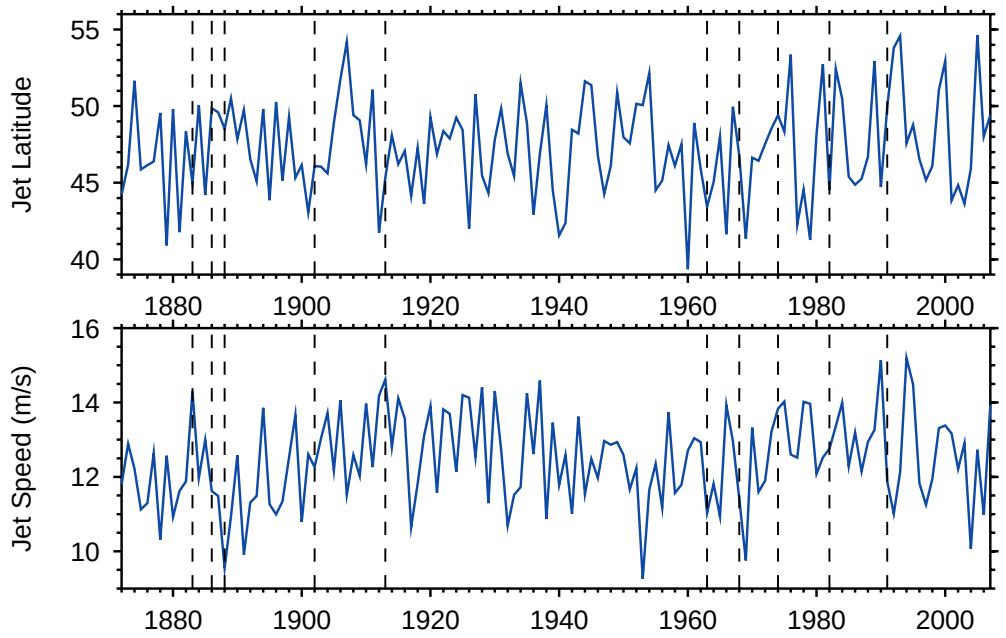


Figure 14: Timeseries for the latitude (°N) and speed (ms^{-1}) of the North Atlantic jet analysed in the regression analysis. The dashed vertical lines show the dates of the 10 eruptions listed in Table 1.

c) Blocking

Blocking frequency is calculated for the period 1948-2010 using the NCEP-NCAR reanalysis. The Absolute Geopotential Height (AGP) method of Scherrer et al. (2006) is used to calculate the blocking frequency from the 500hPa geopotential height field. This blocking index gives a 2D map of blocking frequencies at every grid point. This method identifies a blocking event at a grid point if two criteria are met (as described in Gray et al., 2016):

1. The 500hPa geopotential height gradient in the north-south (meridional) direction is reversed from usual conditions (i.e. the southward gradient is positive, meaning that there is an area of higher pressure to the south, rather than the 'usual conditions' which would be the opposite of this with a negative southward gradient in geopotential height and an area of lower pressure to the south), and

2. The air flow to the north of the grid point is westerly with a height gradient greater than 10m per degree of latitude.

A 5-day persistence criterion is applied to each grid point so that a grid point corresponds to a blocking event only if the above two conditions are satisfied for five or more consecutive days.

In line with Gray et al. 2016, regression analysis of blocking frequency was carried out for the period from 1953-2010 to allow the inclusion of a QBO index in the regression here. Although, as noted previously, the inclusion or exclusion of the QBO term in the regression analysis did not give significant differences in the results. The QBO index used here was derived as in Gray et al. 2016 using equatorial wind radiosonde observations (found at gcmd.nasa.gov/records/gcmd_qbo_zonal_wind_index.html).

Figure 15 shows the climatology and standard deviation of the blocking frequency for the 1953-2010 period (reproduced from Gray et al. 2016). This shows the areas more prone to blocking events around the North Sea and Greenland (typically referred to as high latitude or 'Greenland blocking') which have a high climatological blocking frequency along with high variability, as shown in the standard deviation. Areas of high variability are also seen in areas southeast of the UK and over the Azores.

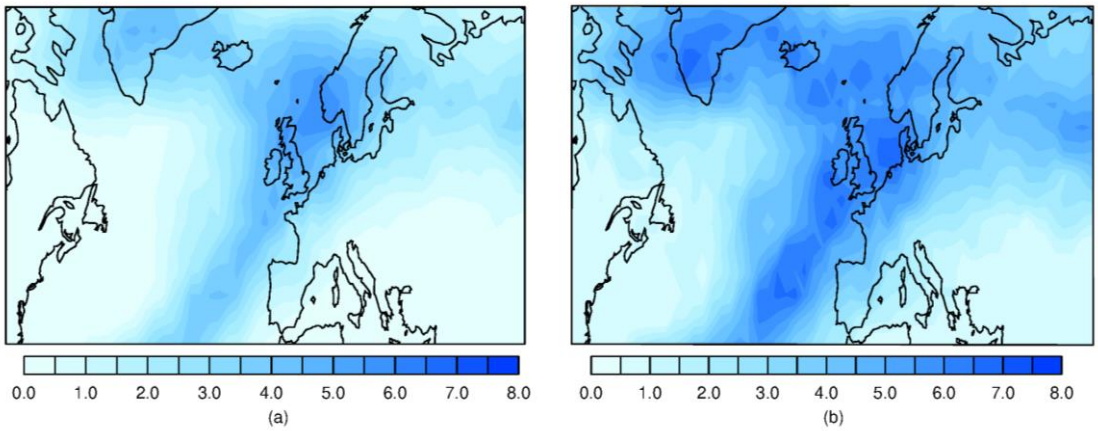


Figure 15: (a) Climatology, and (b) standard deviation of DJF averaged blocking frequency (% per day, or roughly the number of blocked days over the 90-day DJF period) calculated for the 1953-2010 period using the NCEP-NCAR reanalysis (reproduced from Gray et al., 2016).

4. Results & Analysis

The response to large volcanic eruptions in mean sea level pressure, sea surface temperatures, the NAO, the North Atlantic jet, and blocking frequency are assessed here, using the multiple linear regression analysis technique. The results are discussed and compared between the different fields for the different time periods and lags and their consistency is assessed.

4.1 Sea Level Pressure

4.1.1 Regression Analysis

Figure 16 shows the DJF averaged volcanic signal in mean sea level pressure (SLP) over the North Atlantic sector for three different datasets: HadSLP, which is purely observational, and the 20CR and ERA-20C reanalyses. This figure shows these results for various lags from 0 to 5 years and for a time period from 1900-2010. This time interval was chosen to allow a clear comparison between the observational and reanalysis data to validate the reanalyses and assess confidence in further analysis done on fields solely using reanalysis data.

The first row of this figure shows the lag 0 response, which corresponds to the first winter following an eruption. From all three datasets there are significant SLP anomalies indicating a positive NAO phase, which is consistent with results and mechanisms mentioned previously. This is shown by the significant positive SLP anomalies over the North-East Atlantic and Western Europe, peaking at around 5hPa in the HadSLP data, and even larger peak anomalies of almost double that in the reanalysis data, and corresponding significant negative SLP anomalies stretching from the east of Greenland. It is worth noting that whilst these anomalies project onto the positive phase of the NAO, the centres of action of the positive and negative SLP anomalies are shifted slightly northwards of the usual locations used to define the NAO phase (i.e. Iceland and the Azores) and extend eastward across into Europe. The larger responses in

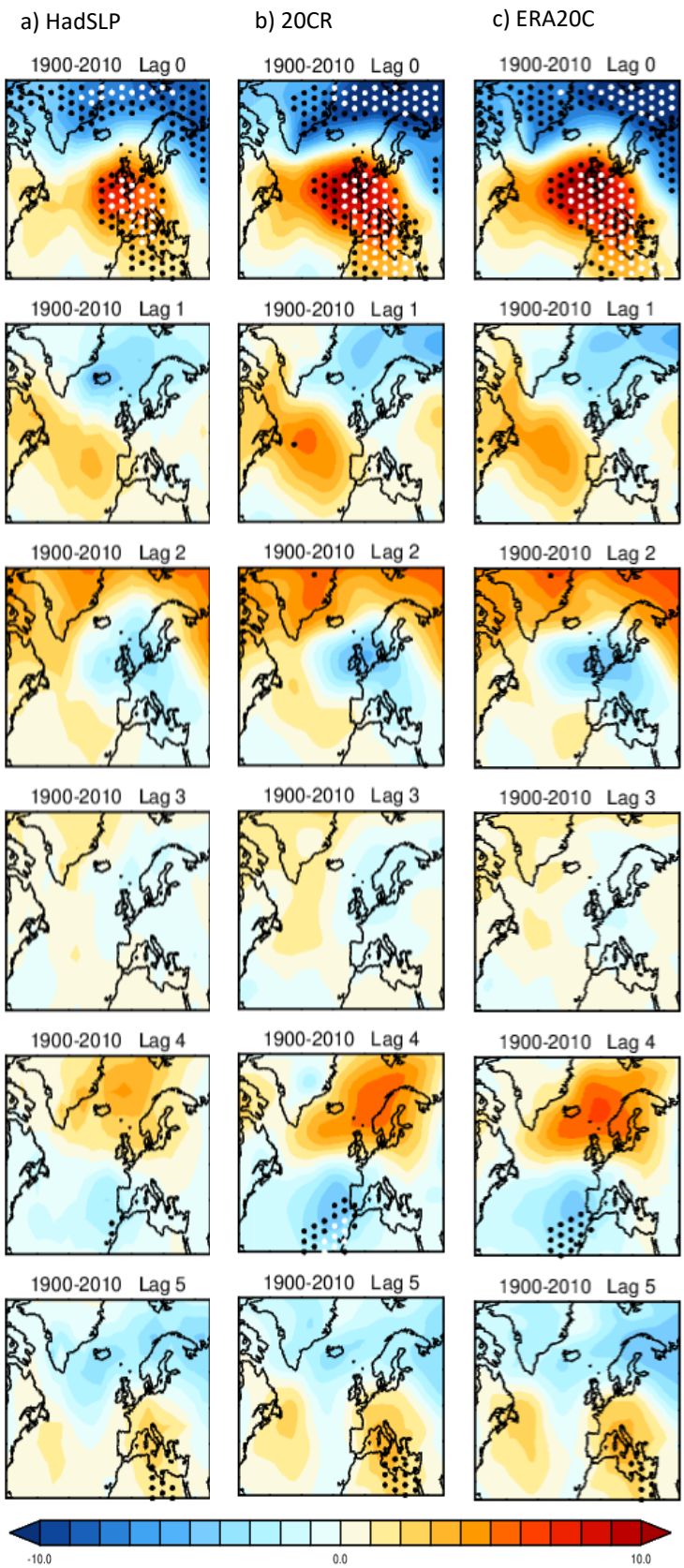


Figure 16: DJF-averaged volcanic response (hPa) from the regression analysis of mean sea level pressure (SLP) from the (a) HadSLP, (b) 20th Century Reanalysis, and (c) ERA20C datasets at various lags from 0 to 5 years for the period 1900-2010. The regression coefficients have been scaled to show the maximum likely response to the largest eruption within the time period (i.e. Pinatubo). Black and white stippling shows regions of 95% and 99% significance respectively.

the reanalysis datasets suggest that while the pattern of response is similar to the observed response, the amplitude may be over-estimated in the reanalyses (or possibly under-estimated in observations due to lack of observations in some areas).

The second row of the figure shows the lag 1 response, which is the 2nd winter following the eruptions. Many previous studies have taken a composite average of the first and second winters following their chosen eruptions when investigating the impact of volcanic eruptions (e.g. Robock, 2000) and this practice has tended to perpetuate (e.g. Driscoll et al., 2012). This was presumably originally done to improve statistical significance, since there is also a positive NAO response at lag 1 year, and the practice has perpetuated the idea that the positive NAO phase caused by an eruption persists for (at least) two years. However, the lag 1 results of the regression analysis here in Figure 16 do not show any significant SLP anomalies at all in any of the datasets, suggesting that the majority of the volcanic response in SLP in fact comes from the first winter alone.

A further interesting result from the regression analysis shown here in Figure 16 is the volcanic response at lag 4 years, i.e. the 5th winter following an eruption. Across all datasets, there is an area of a small negative SLP anomaly centred to the south-west of Portugal with a magnitude of about 2-3hPa at 95% significance, rising to 99% significance for the 20CR results. Although not significant, there is also an area of positive SLP anomalies further north, centred to the east of Iceland. The magnitude of both of these anomalies are larger in the reanalysis dataset results than in the observational HadSLP data (similar to the results at lag 0). The pattern of these anomalies might suggest a weak negative NAO phase at this lag 4 point, implying that the NAO phase has reversed from positive in the first winter to negative by the 5th. However, whether this is a real response needs to be considered since volcanic aerosols only persist in the atmosphere for a couple of years. If this was indeed a real response, the most likely mechanism leading to this would probably involve the oceans since their increased heat capacity means that

surface impacts can potentially persist for a much longer timescale there than in the atmosphere. It is also worth considering whether this 'lag 4 response' is simply an artefact of the regression analysis method used here. For example, the multiple linear regression technique assumes that the timeseries that represent potential influence factors are orthogonal. However, it is well known that El Chichón and Pinatubo both erupted at similar phases of the solar cycle (solar max) so for part of the time interval the volcanic and solar signals are similar. Employing the full 110 years would hopefully avoid this. Indeed, this interference between the solar and volcanic signals was extensively investigated in the solar cycle analysis of Frame and Gray (2010) who concluded that this was unlikely to be a problem. However this issue could benefit from some further investigation beyond this analysis. The presence of this 'lag 4 response' will also be discussed in the results in the following sections.

When comparing the results of the regression analysis of the three datasets, the spatial patterns of the anomalies shown are largely consistent across all three, implying a certain level of confidence in the reanalysis data, although the peak anomalies are somewhat larger in the reanalysis results compared to the observational data results, as previously mentioned. These comparisons appear to be true at all lags.

Figure 17 shows the same as Figure 16, but with the full data for HadSLP and 20CR used, extending the period of regression to 1870-2010. The addition of these first 30 years, which spans the very large eruption event of Krakatau, slightly weakens the anomalies at lag 0 and strengthens them at lag 1, now giving some significant positive SLP anomalies at lag 1 year over the north Atlantic in the HadSLP and 20CR results of around 3-5hPa at the peak (although it is still not a typical NAO distribution). The response at lag 4 showing the reversal in the NAO pattern is also now significant here. This implies that adding the time period including the Krakatau eruption has a relatively important influence on the regression results.

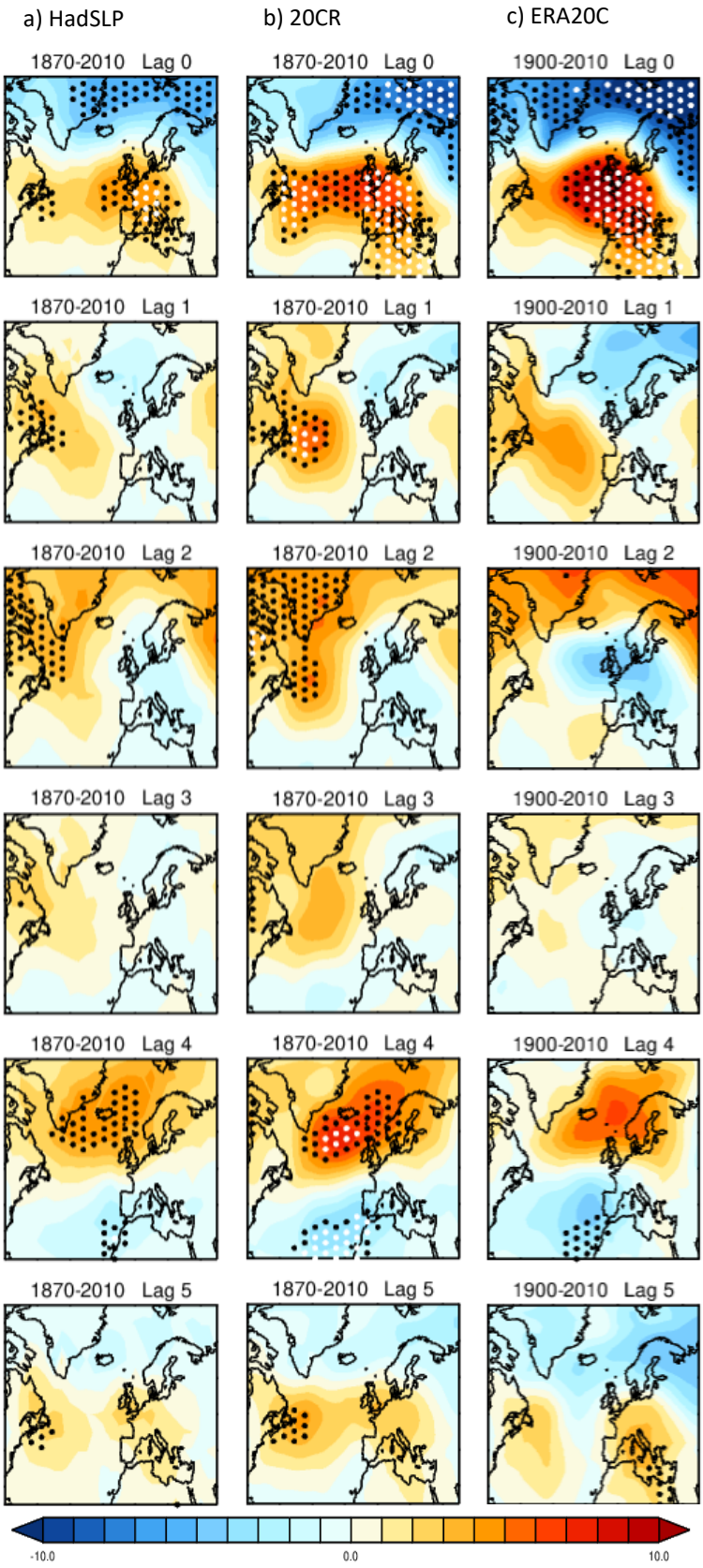


Figure 17: As Figure 16, but at various lags from 0 to 5 years for the period 1870-2010 (columns (a) and (b)) or 1900-2010 (column (c)).

To further investigate the impact of including or excluding selected time periods, the regression analysis has been repeated using different time periods that centre on different groups of eruptions.

Figure 18 shows the same as Figure 17, but now splitting up the regression time period into 30-year periods centred on groups of eruptions. As described in Section 3.4, four time intervals are chosen: 1870-1900 (which includes Krakatau, Tarawera, and Bandai), 1900-1930 (which includes Santa Maria and Colima), 1950-1980 (which includes Agung, Fernandina, and Fuego), and 1980-2010 (which includes El Chichón and Pinatubo). The first and second winter responses are focussed on here, i.e. lag 0 and lag 1. Here, you can see that the strongest responses in all three datasets are coming from the most recent time period of 1980-2010, which shows significant positive and negative anomalies of around +/-10hPa respectively, each at 99% significance. This period includes the eruptions of El Chichón and Pinatubo, both of which are very large compared to some previous eruptions (as seen in the volcanic aerosol timeseries in Figure 10). In fact, the pattern of the response shown in this later period is very similar to the overall pattern shown in Figure 16 when considering the full time period from 1900-2010, suggesting that these recent eruptions have a large influence over the whole period. However, this is not the only thing influencing the whole period results as it was shown in Figure 17 that including the early 30 years for the HadSLP and 20CR data did in fact change the results of the regression analysis. However, the patterns still remain very similar to the results from the 1980-2010 period. The way that the signal changes depending on the period chosen for the regression analysis is also found when looking at the solar signal (e.g. Gray et al., 2016), suggesting possible nonlinear processes or a nonstationary response to both solar and volcanic forcing. Despite this, in Figure 18 you can still see that the response from the first post-eruption winter (lag 0) is a lot stronger and more significant than that in the second winter (lag 1) in all time periods and datasets, which is consistent with results presented in Figures 16 and 17.

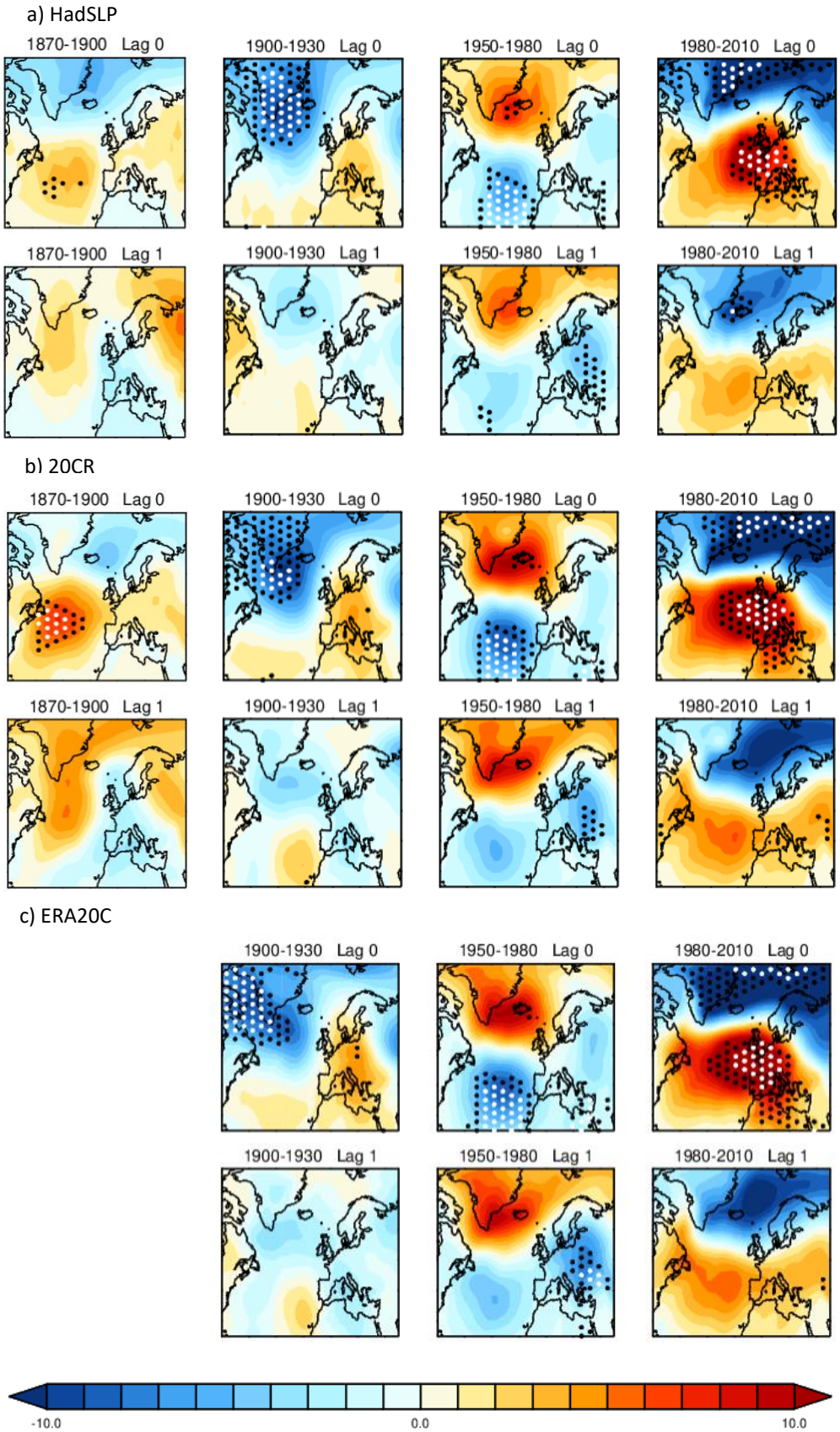


Figure 18: As Figure 17, but at lags of 0 and 1 years for various time periods between 1870-2010.

One interesting feature to note from Figure 18 is that the response shown in the regression analysis for the period 1950-1980 that includes the Agung eruption seems to be somewhat the opposite in pattern to all other time periods, including the full regression periods. In all three datasets, the SLP anomalies shown for 1950-1980 indicate a negative NAO pattern, with a strongly significant negative SLP anomaly centred over the Azores and a slightly significant positive anomaly centred over Iceland. This is clearly the opposite of the positive NAO pattern shown in the response for all other time periods and the full period, as well as many previous results when analysing the response to volcanic eruptions. However, if we look at the largest eruption during that time period, which was that of Agung in 1963, it has been shown that there was in fact a negative NAO index in that first winter following the eruption (e.g. Wunderlich and Mitchell, 2017), consistent with the results shown here.

When comparing the three datasets, again we can see consistency in the patterns and significance of the anomalies shown, however the magnitude of the anomalies are again larger in the reanalysis data results.

4.1.2 Composite Analysis

As a comparison to the above regression analysis, and as a test against the methods used by previous studies, a brief composite analysis was carried out on the same three SLP datasets. Here, the composite averages were taken for the post-eruption winters following the largest eruptions (according to the volcanic aerosol data used here) for the period common to all three datasets: 1900-2010. This gave 7 eruptions, namely Santa Maria, Colima, Agung, Fernandina, Fuego, El Chichón, and Pinatubo, with eruption dates given in Table 1. As two of the eruptions, Santa Maria and Fuego, occurred in the October of their respective eruption years, the first winter used in the composite analysis was in fact that of the second post-eruption year to allow for the atmospheric response to the eruptions to build. This convention for defining the post-eruption winters has also been used in previous studies, e.g. Driscoll et al. (2012). The anomalies

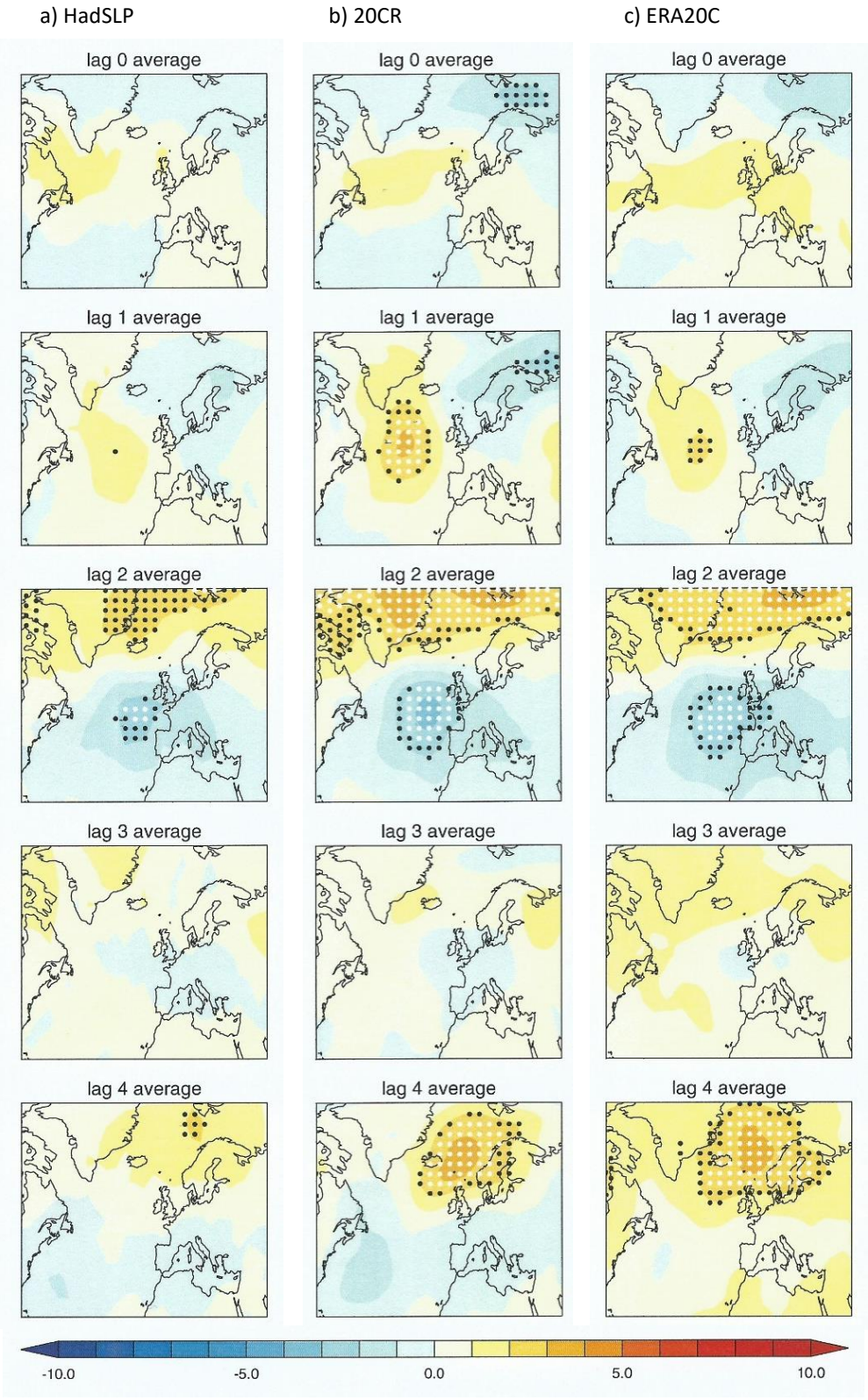


Figure 19: Composite anomalies in mean sea level pressure (hPa) during the winters following the 7 largest volcanic eruptions between 1900-2010 (see Table 1) from the a) HadSLP, (b) 20th Century Reanalysis, and (c) ERA20C datasets. The average is shown for individual post eruption winters from the first (lag 0) to the fifth (lag 4). Black and white stippling shows regions of 90% and 95% significance respectively.

in SLP were calculated from the climatology of the entire 1900-2010 period and significance values were calculated using a 2-sided t-test, as with the regression analysis (although in this case, regions of 90% and 95% significance are shown on the figures as there were no regions over 99% significance). As with the regression, individual post-eruption winters are shown separately, from the first (lag 0) to the fifth (lag 4), as opposed to averaging over the first and second winters.

The results for this composite analysis are shown in Figure 19. The first winter composites shown in the top row of the figure do not show any particularly significant patterns of anomalies, with the only region above 90% significance being a small area of a negative SLP anomaly north of Norway, which only appears in the 20CR results. However, the pattern and sign of the SLP anomalies are similar to those shown in the regression, although much weaker and not significant here. The lag 1 (2^{nd} winter) averages show a similar trend, with the pattern and sign of the anomalies being similar to those shown in the regression, but much weaker and much less significant. Here, there are slightly more significant anomaly regions than at lag 0, mainly an area of weak positive SLP anomalies over the North Atlantic, although this only reaches 95% significance in the 20CR data.

These composites appear to be relatively consistent with previous studies, although it is difficult to comment on a direct comparison since previous studies tended to average over the first two winters following an eruption rather than showing the winters individually, as is done here. However, the general patterns and peak magnitudes of anomalies shown here seem consistent if you look at the first two winters, for example when comparing to Driscoll et al. (2012) who also looked at composites of 20CR data and took an average over a similar set of eruptions (namely Krakatau, Tarawera, Bandai, Santa Maria, Quizapu, Agung, Fuego, El Chichón, and Pinatubo), although they extended slightly further back in time.

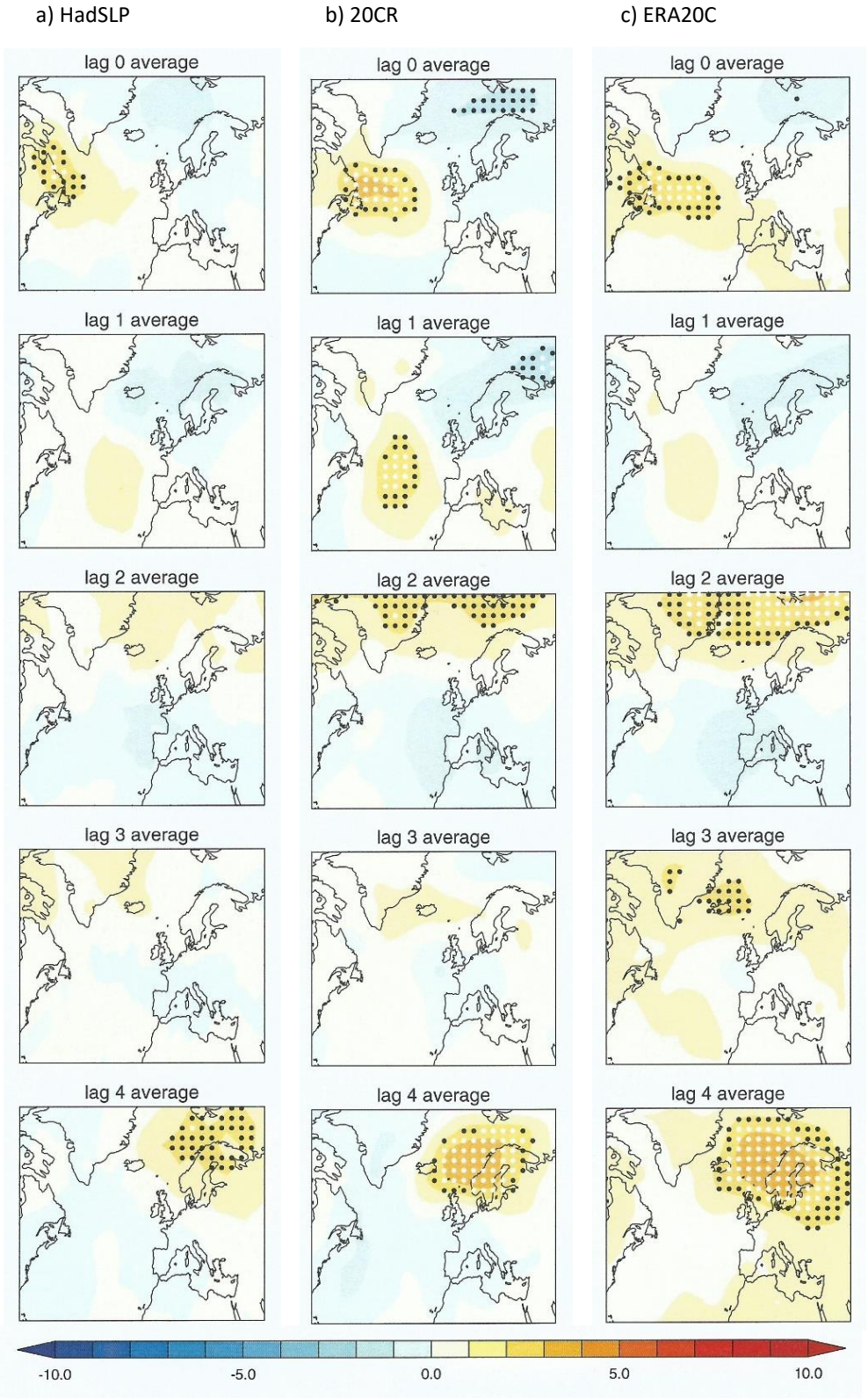


Figure 20: As Figure 19, but with the winters following the Agung eruption in 1963 removed.

The largest and most significant response shown here seems to appear at lag 2 according to these composites, which was not shown at all in the regression and seems a little suspicious. The composites are also picking up a slight 'lag 4 response', again similar in pattern and sign to that shown in the regression.

Interestingly, if you remove the winters following the eruption of Agung from the composites, this significantly changes the results. This is shown in Figure 20. Now, there is a 95% significant SLP anomaly pattern appearing in the first winter, again similar to that shown in the regression indicating a positive NAO phase, although small in magnitude here with peak positive anomalies of only around 2-3hPa. These are also more significant here than in the second winter, like in the regression results. Removing Agung from the composites has also weakened the slightly spurious lag 2 anomalies, however significant anomalies at lag 4 still remain, although again only peaking at 95% significance. This further suggests that the response to the Agung eruption was different to the others, as was shown in the regression results.

In summary, the composites shown here do not show many very clear strong or significant signals in the first 2 winters following an eruption, giving reasonable justification for using a method like multiple linear regression analysis to separate the impact of other forcings so as not to hide any underlying volcanic response.

4.2 Sea Surface Temperature

Figure 21 shows the DJF averaged volcanic signal in sea surface temperature (SST) over the North Atlantic sector, comparing the regression results from the observational HadISST dataset to the ERA-20C reanalysis dataset for the period 1900-2010 at lags from 0 to 5 years (there was no SST output field available for the 20CR reanalysis). Similarly to the SLP results, there is good agreement between the two datasets at all lags, with the size of the SST anomalies being once again slightly larger from the reanalysis data.

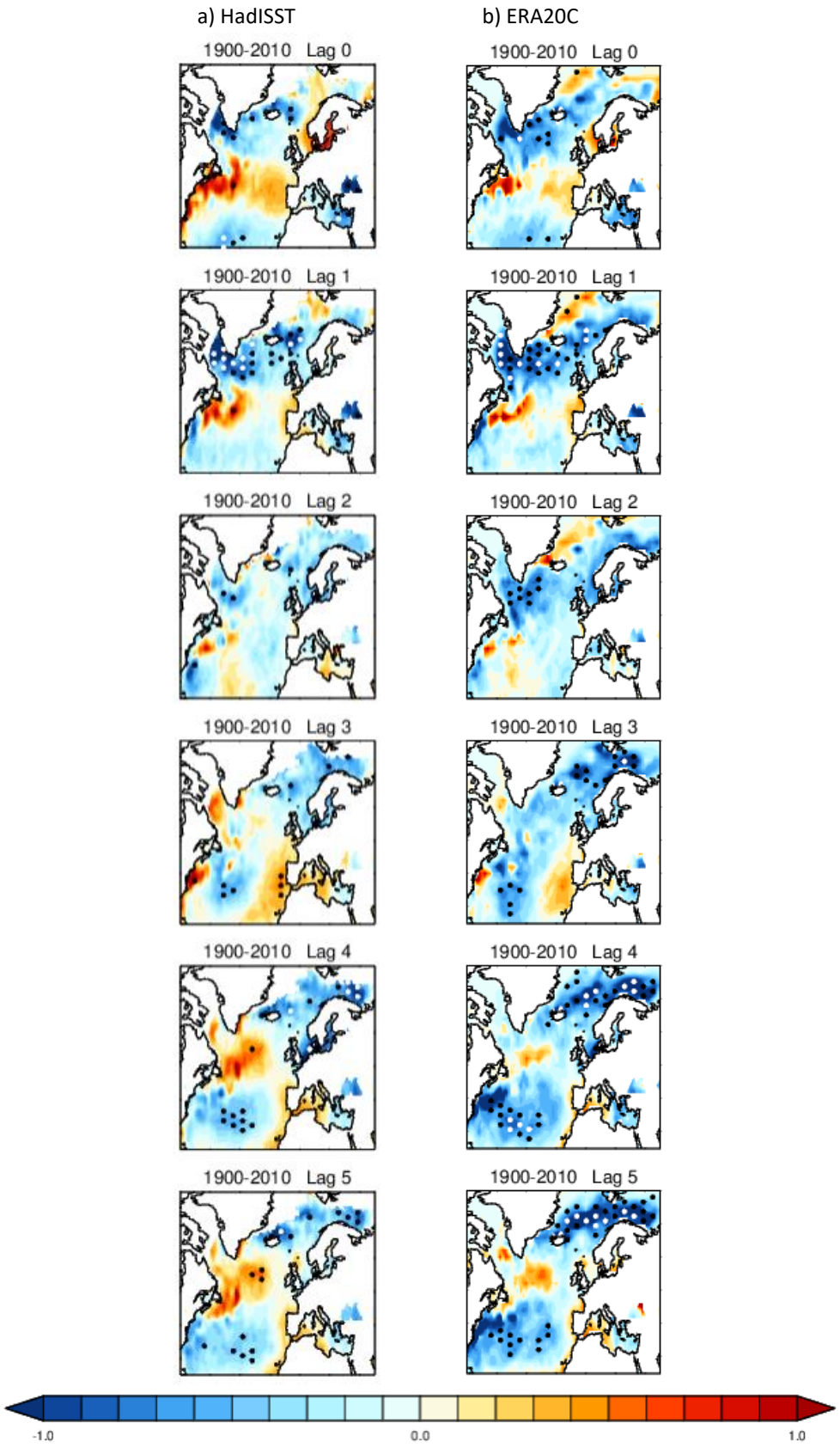


Figure 21: DJF-averaged volcanic response (K) from the regression analysis of sea surface temperature (SST) from the (a) HadISST, and (b) ERA20C datasets at various lags from 0 to 5 years for the period 1900-2010. The regression coefficients have been scaled to show the maximum likely response to the largest eruption within the time period (i.e. Pinatubo). Black and white stippling shows regions of 95% and 99% significance respectively.

The tripolar anomaly structure in the lag 0 response shown in the first row appears consistent with the results shown for SLP, with the pattern of the SST anomalies being what you would expect from a positive NAO phase (e.g. Hurrell et al., 2003). However, whereas in the SLP results the response at lag 0 was much stronger and more significant than that at lag 1, the opposite is true here, with the volcanic response in SSTs being much more significant at lag 1 than at lag 0. The higher heat capacity of the oceans means that an ocean response is likely to perpetuate for longer than the corresponding atmospheric response, but it also suggests the possibility that the response in SST actually builds from the first winter into the second winter following an eruption.

A significant 'lag 4 response' can also be seen, which again appears to be a slight reversal of the anomaly pattern from the first and second winters (lag 0 and lag 1). Unlike in the SLP results however, this lagged response persists into the following winter at lag 5, again suggesting that the ocean signal perpetuates for longer and that the lag 4 atmospheric response may be in response to the longer-term ocean response.

Including the first 30 years of available observational SST data, as shown in Figure 22 appears to increase the significance of the anomalies at all lags, particularly at lag 0, in contrast to the SLP results which were weakened by including these years. The inclusion of these years also greatly increases the significance of the 'lag 4 response' anomaly pattern, increasing much of the areas of positive and negative SST anomalies to 99% significance, which was also seen for the SLP results in Figure 17.

The volcanic response in shorter time periods centred around groups of eruptions was also analysed as with SLP and is shown in Figure 23. As with the response in SLP (Figure 18), the volcanic response in SST at lag 0 appears dominated by the most recent time period spanning 1980-2010, but also in this case by the early period from 1870-1900, which as mentioned previously covers the eruption of Krakatau. These two periods show similar patterns in

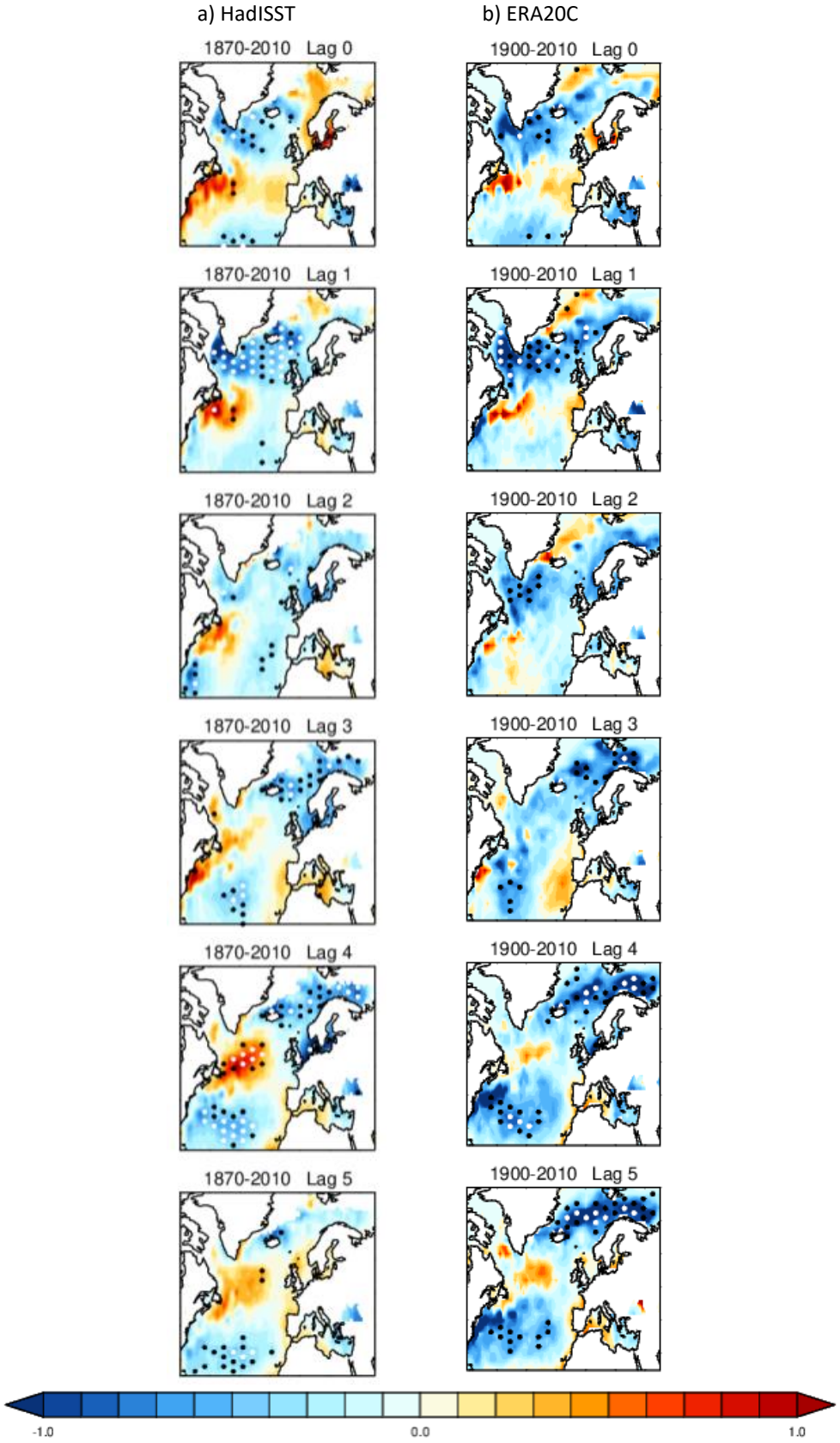


Figure 22: As Figure 21 but at various lags from 0 to 5 years for the period 1870-2010 (column (a)) and 1900-2010 (column (b)).

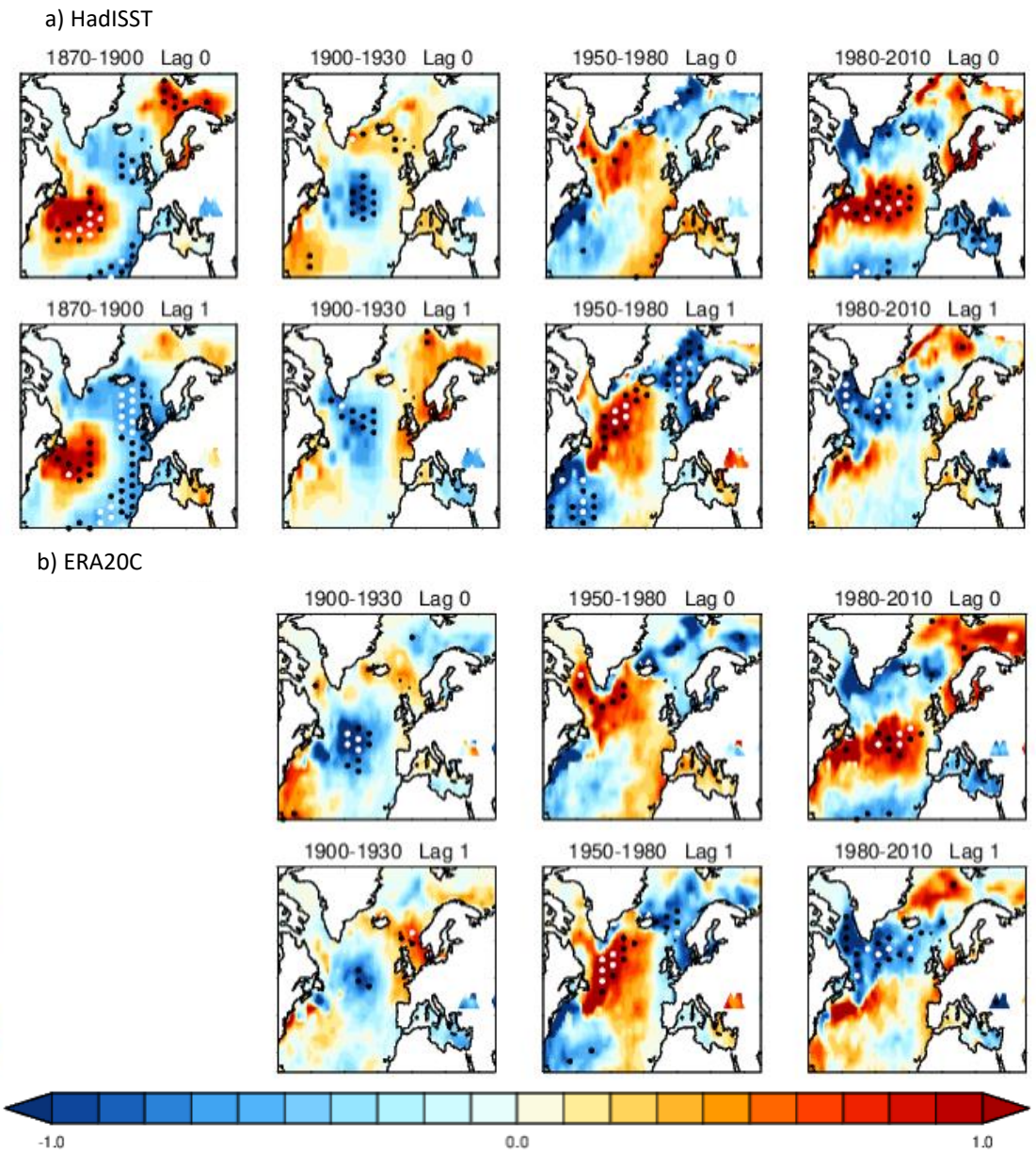


Figure 23: As Figure 22, but at lags of 0 and 1 years for various time periods between 1870-2010.

significant SST anomalies. Again, the response pattern seems somewhat reversed for the 1950-1980 (Agung) period, as was also seen in the SLP response.

In summary, the volcanic response in SSTs remains consistent with the results presented previously for SLP, showing a similar positive NAO related pattern in the first and now second winter, suggesting that this response might build in the oceans. The reversed 'lag 4 response' can also be seen in this field, and when looking at smaller time periods, the response again

seems to be somewhat dominated by the eruptions of El Chichón and Pinatubo during the 1980-2010 period, and the response for 1950-1980 seems to be the opposite pattern.

4.3 The NAO & the North Atlantic Jet

4.3.1 The NAO Index

To double check the patterns shown in the volcanic response in SLP and SST which imply positive NAO phases in the first and possibly second winters following an eruption, a similar regression analysis was carried out on a simple NAO index (as described in Section 3.5.1) giving the volcanic response for the entire period from 1870-2010, as well as the shorter time periods. These results are shown in Figure 24. Here, the significance values at each lag are displayed above the corresponding bar chart, rounded to two significant figures.

Overall, the regression results for the NAO index are happily consistent with the SLP and SST results. Whilst the responses shown at lag 0 do not actually show any signals above the 95% significance level for any of the time periods, they are however the correct sign corresponding to the patterns shown in the SLP and the SST results (i.e. positive NAO index anomalies for all periods except 1950-1980). This is likely due to the definition used for the NAO index here (again, as described previously in Section 3.5.1) since the sites used to define the pressure differences are Iceland and Gibraltar, and the anomaly patterns shown in the SLP responses for example appear to be shifted slightly to the north and eastward of these locations so that the regression patterns do not project well onto the NAO. The NAO index response also shows a decrease in the size of this anomaly at lag 1, although still of the same sign as at lag 0, and which is less significant, also consistent with the SLP results.

These results for the NAO index appear consistent with previous studies that have looked specifically at the NAO index following eruptions, for example Swingedouw et al. (2017). In their analysis, they used the same definition of the NAO index and took a composite value averaged

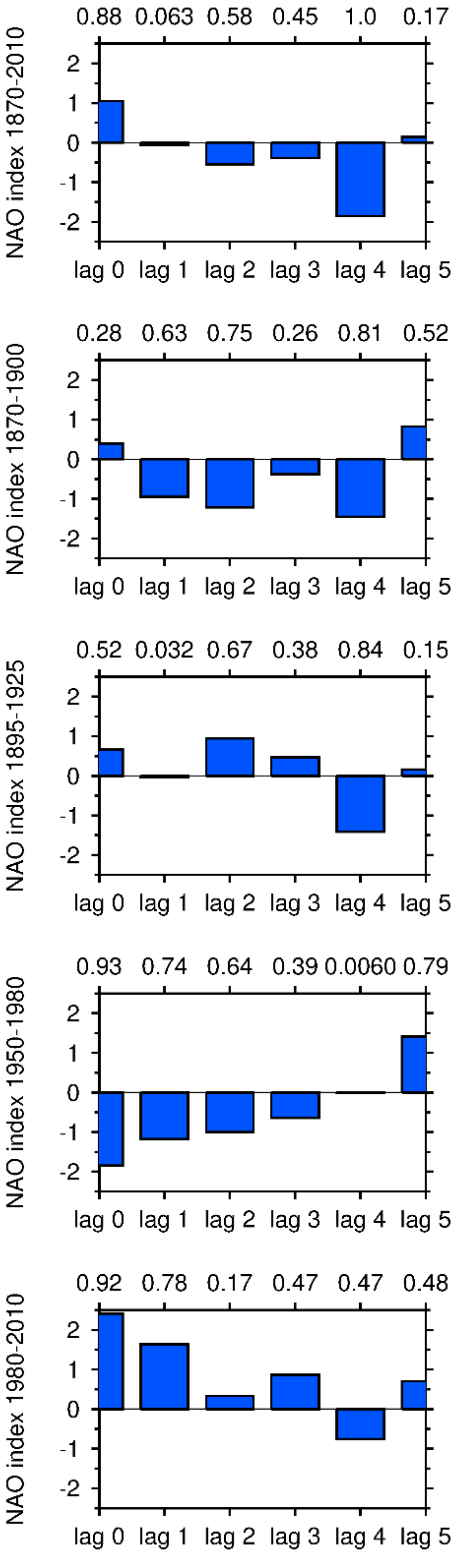


Figure 24: DJF-averaged volcanic response from the regression analysis of the NAO index (see Section 3.5.1) at various lags from 0 to 5 years for various time periods between 1870-2010. The regression coefficients have been scaled to show the maximum likely response to the largest eruption within the time period (i.e. Pinatubo). The significance values from the two-sided Student's t-test are shown above each plot, rounded to 2 significant figures.

over the 5 largest eruptions since 1870 (Krakatau, Santa Maria, Agung, El Chichón, and Pinatubo) for each winter up to 5 years following the eruptions. They too found only a weak positive NAO index anomaly present in the first 2 winters which was not significant at the 90% level. They also did the same analysis using an NAO index derived from the first empirical orthogonal function (EOF) in SLP over the North Atlantic using 20CR data, which showed the same result. It could be worth using a similarly defined NAO index to compare to results shown here to see whether using the EOF definition improves the significance of the results. However, the results here are still consistent with those shown in the responses in SLP and SSTs, and are largely consistent with the proposed mechanisms.

Similarly to the results for SLP and SST, the volcanic response in the NAO index for the whole period shows a significant and strong negative NAO index anomaly at lag 4, showing this reversed 'lag 4 response' from the initial positive NAO phase. However, although the reversed response is seen in three of the four shorter time periods the response is not significant above the 95% significance level in any of them.

4.3.2 Jet Latitude & Speed

The proposed dynamical mechanisms following volcanic eruptions suggest that stratospheric aerosol heating leads to a strengthened polar vortex (see Section 2.2), which is known to affect wave propagation in the troposphere and influence the winds and the jet stream here. It has been seen that the tropospheric jet tends to move polewards when the stratospheric polar vortex is stronger, and equatorwards when the polar vortex is weaker (Baldwin and Dunkerton, 1999). Therefore this might suggest that volcanic eruptions would have an impact on the North Atlantic jet stream, particularly the latitude and possibly the speed of the jet. This is also supported by the findings of some modelling studies investigating the impact of volcanic aerosol induced stratospheric heating on the jet which also find an implied poleward shift (e.g.

DallaSanta et al., 2019). This is investigated in this section through some further regression analysis.

Figure 25 shows the DJF averaged volcanic signal in jet latitude and speed at various lags from 0 to 5 years, and for various time periods between 1872-2007, aligned with previous analysis and figures. Looking at the entire time period available here (1872-2007), the results show a significant positive anomaly in jet latitude at lag 0 which is greater than 99% significant. This implies a poleward shift of the jet in the first winter following an eruption, which is consistent with the proposed mechanisms described above.

When looking at the shorter time periods, it seems that the results are again dominated by the recent 1980-2010 period, which also shows a highly significant positive anomaly in jet latitude with about twice the magnitude of the anomaly for the entire period. However, the other time periods do not show a consistent positive latitude anomaly, although none of these other time periods have a response above 95% significance. Furthermore, there are no significant anomalies at lag 1 (the 2nd winter), similar to the results for SLP and the NAO index, suggesting again that the majority of the volcanic signal in these atmospheric phenomena comes from the 1st winter. There are also no significant anomalies at lag 4 for any time periods here, showing no 'lag 4 response' in the jet latitude.

The volcanic response in jet speed shows no highly significant anomalies at lag 0 or lag 1, suggesting there is no initial impact of an eruption on the speed of the jet. However, there are some large and highly significant negative anomalies at a lag of 4 years, suggesting a decrease in the speed of the jet at this lag. This lag 4 weakening of the jet appears to be the most robust feature when looking at the response in the jet here, and is most pronounced when looking at the entire period from 1872-2007, which shows a strong negative anomaly of over $2ms^{-1}$ at above 99% significance. A negative jet speed anomaly appears at this lag in all other time

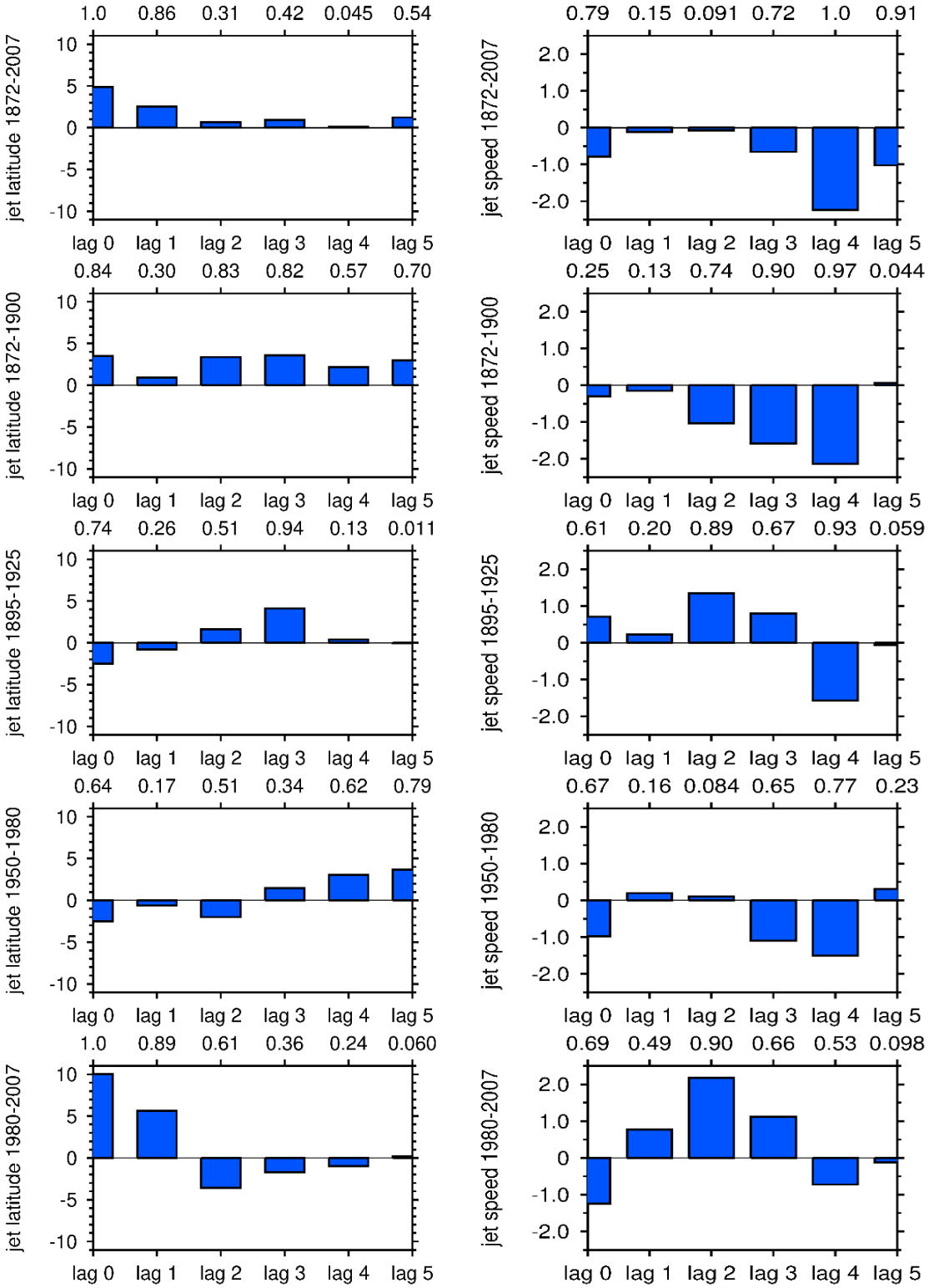


Figure 25: As Figure 24, but for the jet latitude (degrees) and jet speed (ms^{-1}) indices calculated from the 20th Century Reanalysis dataset (as described in Section 3.5.2) at various lags from 0 to 5 years for various time periods between 1872-2007.

periods, although this is only above 95% significance for the 1872-1900 period. This lagged response in the jet speed suggests there might be a different mechanism at play here to the one affecting the polar vortex and jet latitude, possibly through an ocean response, and which is likely related to the 'lag 4 response' found in the other fields analysed (SLP, SST, and the NAO index). This could also suggest some form of inter-decadal coupling with multi-decadal variations of the jet speed (Woollings et al., 2015). On the other hand, it could possibly also be an artefact of the regression method and not caused by the eruptions at all, as already discussed. Further research is needed to investigate this lagged response in more detail.

When considering the jet characteristics and the NAO, Woollings et al. (2010a) find that to describe the jet, you need to consider not just the NAO, but also the East Atlantic (EA) pattern, as changes in both of these patterns describe changes in the jet latitude and speed. The EA pattern being referenced here is usually defined as the 2nd EOF of SLP over the North Atlantic (with the NAO being the 1st EOF). They find that a positive NAO combined with a negative EA pattern produces positive jet latitude anomalies (i.e. a poleward shift), and that a negative NAO mainly produces negative jet latitude anomalies. They also find that the jet speed is at its lowest values for both negative NAO and EA patterns. To check whether the jet latitude and speed anomalies shown in the regression analysis are consistent with the results for the NAO index and SLP, it would be a good idea to check the value of the EA index in the winters following the volcanic eruptions. As a quick check, data for the EA index available from NOAA for years from 1950 to the present day (available at: ftp://ftp.cpc.ncep.noaa.gov/wd52dg/data/indices/ea_index.tim) is shown in Table 1 for corresponding eruptions from 1950. The EA index in the first winter following all of these eruptions is negative, proving consistent with combining with the positive NAO (in both the NAO index and SLP analysis) and the poleward shift of the jet.

4.3.3 850hPa Zonal Winds

To take a further look at the impact on the jet and to see this spatially rather than simply through an index, similar regression analysis was performed on 850hPa zonal wind (u) data taken from ERA-20C. This is shown in Figure 26. The contours in the images in the figure show the climatology in zonal wind for that particular regression period.

The results of this regression analysis appear to be largely consistent with the results for the jet latitude and speed indices calculated previously, which used data taken from the 20CR dataset. Looking at the whole available period (1900-2010), shown in the far-left column of the figure, a northward shift in the position of the jet is apparent at lag 0, shown by the area of highly significant (over 99%) positive u anomalies to the north of the climatological jet position with corresponding significant negative anomalies to the south of these positive anomalies. Again, similar to the volcanic response shown in other fields, this appears to be dominated by the most recent regression period from 1980-2010, and the 1950-1980 period shows a somewhat opposite pattern. Furthermore, the major response is from this first winter (lag 0), with few significant regions of anomalies at lag 1, consistent with other results presented in this section.

Looking in more detail at the 1950-1980 period here, the jet speed during this time seems to be noticeably larger than other periods, and the centre of the jet is located further poleward. This could potentially have an impact on the vertical coupling between the stratosphere and the troposphere and could possibly explain the opposite signed signal seen during this time period in other fields during the time of the Agung eruption. This could be further investigated.

Looking at lag 4 for the entire period, a 95% significant response can also be seen here, with a region of negative u anomalies close to the region shown in the climatology of maximum u speeds. This implies a potential decreasing of the jet speed, which would be consistent with the results presented in Figure 25 when looking at the volcanic response in the calculated jet speed

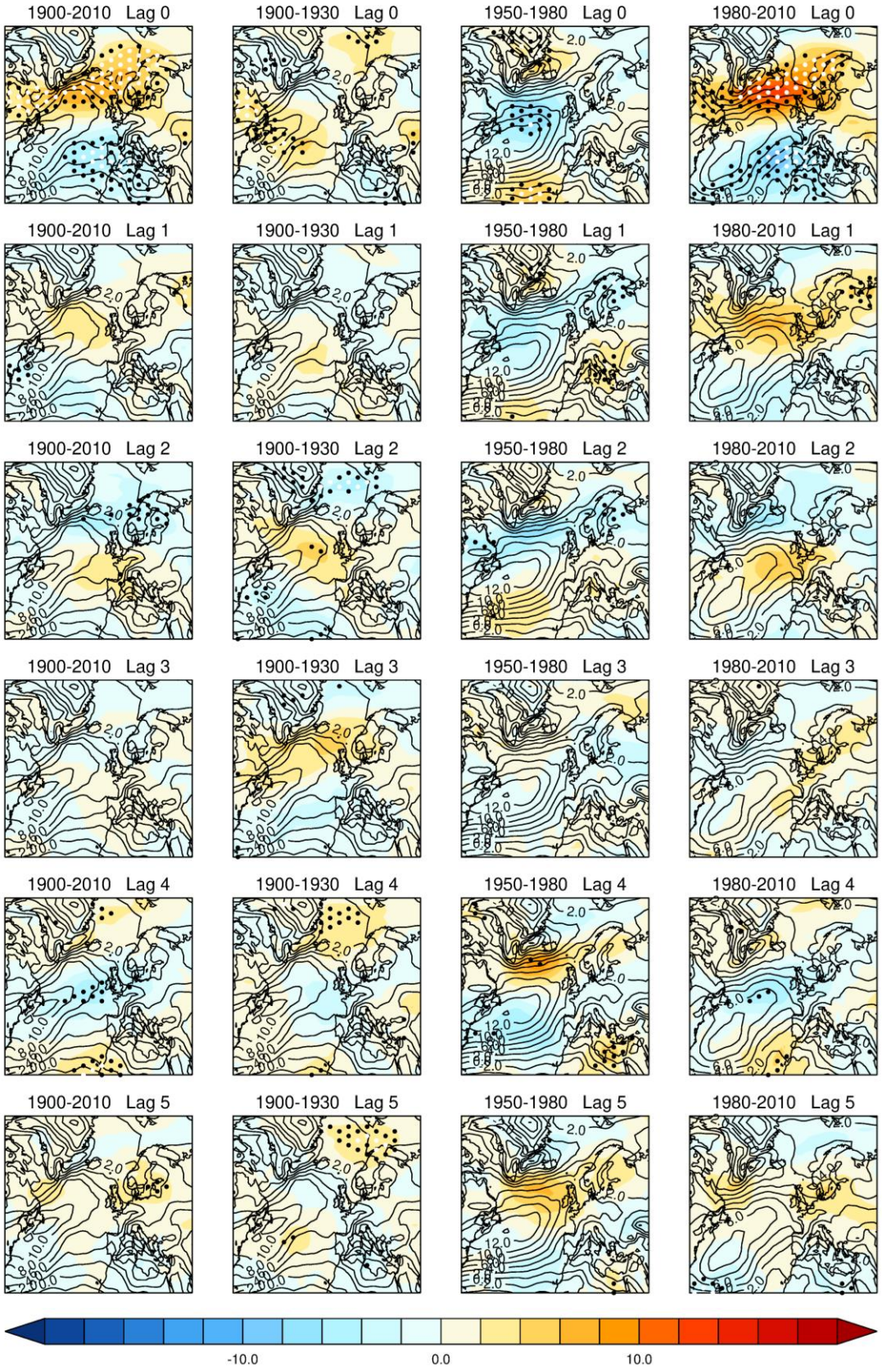


Figure 26: DJF-averaged volcanic response (ms^{-1}) from the regression analysis of the 850hPa zonal wind from the ERA20C dataset at various lags from 0 to 5 years for various time periods between 1900-2010. The regression coefficients have been scaled to show the maximum likely response to the largest eruption within the time period (i.e. Pinatubo). Black and white stippling shows regions of 95% and 99% significance respectively. The climatology for the zonal wind for each time period is shown in the contours.

index. This effect is not seen as strongly in the other shorter time periods, again consistent with Figure 25.

It is worth noting here that the jet indices calculated to represent the speed and latitude of the jet are somewhat simplistic as they average over the North Atlantic area to pick out a single location of maximum jet speed (as described in Section 3.5.2). As a result, the indices do not take into account many possible features of the jet such as a tilt in the jet, for example the South West-North East tilt seen in Figure 26 here, particularly at lag 0. This is another reason why any changes in jet latitude and speed shown in Figure 25 might appear slightly different to Figure 26 due to the spatial variations of the jet, however they do seem to be rather consistent.

4.4 Blocking

Several studies have found links between atmospheric blocking events and variability within the stratosphere (e.g. Woollings et al., 2010b), as well as an association between increased blocking frequency in certain areas of the North Atlantic sector and the phase of the NAO during winter (e.g. Scherer et al., 2006, Woollings et al., 2008). Clearly, this suggests the possibility of an influence of volcanic eruptions on blocking frequency and persistent blocking events over the North Atlantic sector. In particular, the influence of the stratosphere on blocking, rather than the reverse, might come into play here. This type of mechanism, whereby the stratosphere leads blocking events, has been suggested by Woollings et al. (2010b) for example, who found correlations between the stratosphere and blocking when the stratosphere was leading the blocking, and found that this produced patterns of blocking events associated with a negative NAO phase, namely increased high latitude blocking over Greenland. Gray et al. (2016) also found a solar cycle variation in the frequency of blocking events over the Atlantic and associated this with the 11-year solar variation in stratospheric sudden warming events. It has also been suggested that an increase in blocking over Western Europe and a decrease in blocking over Greenland is associated with a positive NAO phase (Scherer et al., 2006).

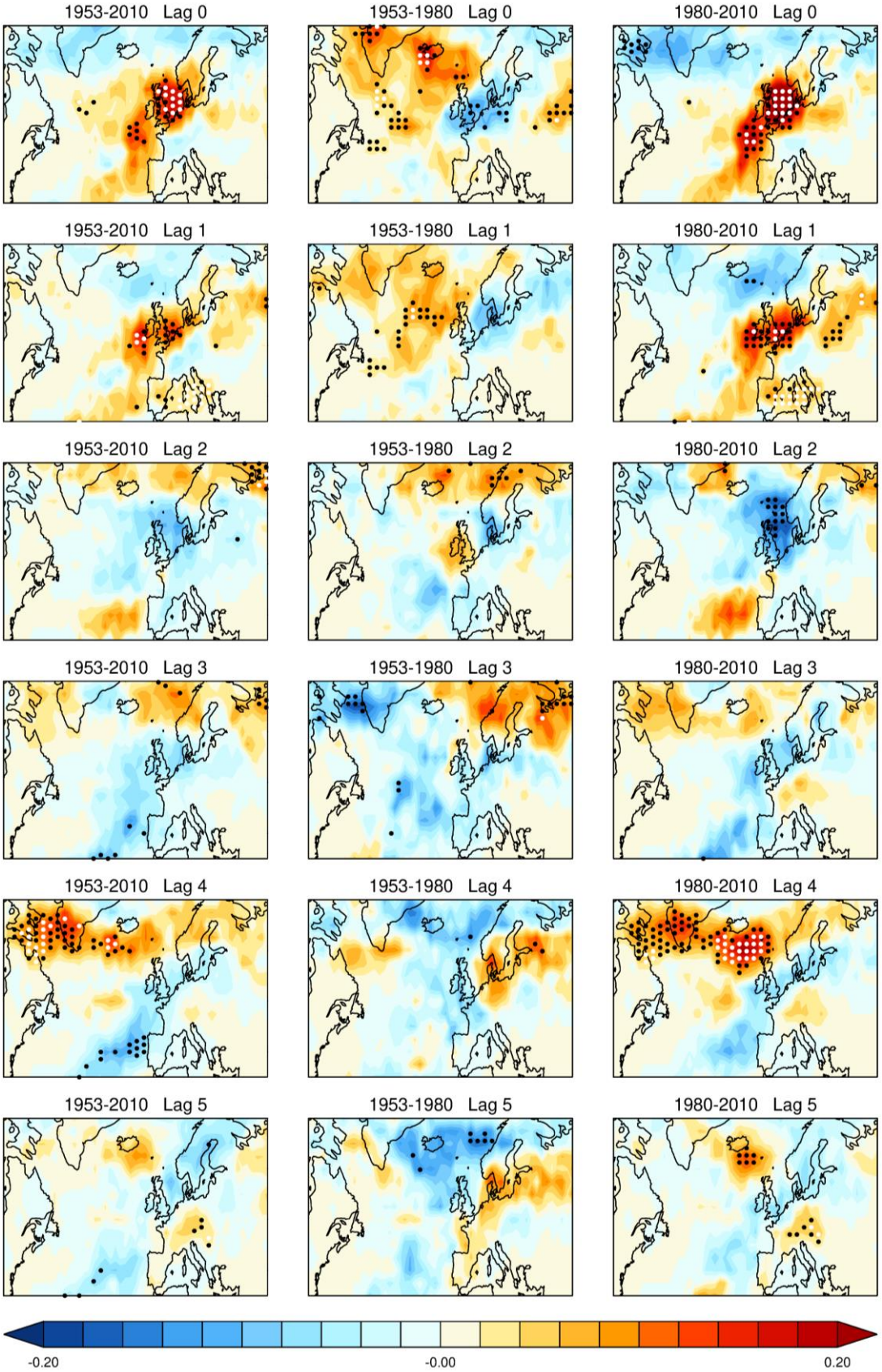


Figure 27: DJF-averaged volcanic response (per day) from the regression analysis of blocking frequency (calculated as in Section 3.5.2) at various lags from 0 to 5 years for various time periods between 1953-2010. The regression coefficients have been scaled to show the maximum likely response to the largest eruption within the time period (i.e. Pinatubo). Black and white stippling shows regions of 95% and 99% significance respectively.

To investigate any potential volcanic influences on blocking, a similar regression analysis was carried out on an index representing blocking frequency, calculated as described in Section 3.5.2. The results of this are shown in Figure 27, which shows the DJF averaged volcanic response in blocking frequency for periods between 1953-2010, again at various lags. For this somewhat shorter period, there are highly significant anomalies in blocking frequency at a lag of zero years. Here, there is a region of significant positive anomalies over the North Sea region, extending slightly over the UK and towards mainland Europe, indicating an increase in blocking over this region. This appears to persist slightly into the second winter (lag 1) although the region decreases in both size and significance. This pattern is somewhat consistent with blocking patterns found to be associated with a positive NAO phase, in line with results presented previously for other analysed fields. Again, as with previous results in this section, this atmospheric response appears to be dominated by the most recent time period (1980-2010), which shows even more significant positive anomalies in blocking frequency over this area. Also again, the period from 1953-1980 seems to show a slightly opposite pattern.

A 'lag 4 response' also seems to be present in the blocking results here, which show an area of significant positive blocking anomalies over the north of the sector, over Greenland. As mentioned previously, this pattern is associated with the appearance of a negative NAO phase, which seems very consistent with the other 'lag 4 response' patterns seen in other fields discussed here and may be associated with a lagged ocean response. This pattern is even stronger when looking at the 1980-2010 period, which again appears to dominate here.

Results for the blocking here do suggest a possible influence of volcanic eruptions on blocking events. The exact mechanism behind this influence could benefit from being explored further to really see how all these influences link together, in addition to further investigation into the 'lag 4 response' shown here as well as in other fields.

5. Summary & Further Work

In this study, the response to volcanic eruptions has been investigated in several fields, namely sea level pressure, sea surface temperature, the NAO, the North Atlantic Jet, and atmospheric blocking. The focus has been on the wintertime response (DJF) in the North Atlantic sector. This is consistent with previous studies which have focused on this region during the winters following strong volcanic eruptions. To complement previous studies, here, a multiple linear regression method of analysis was used to separate the influence of these volcanic eruptions from other modes of climate variability, e.g. ENSO, as opposed to simply looking at composite averages in winters following eruption years. A comparison of observational and reanalysis data was also done for SLP and SST to try to validate the use of reanalysis data for analysing other fields, and these results were found to be largely consistent with those using the observational data.

Overall, this study has found a pleasing level of consistency with previous study results, particularly with the findings of a positive NAO phase in the winter immediately following a strong volcanic eruption which persists into the second winter, although here this persistence was not found to be particularly significant with the strongest responses being shown in the first winter. This suggests that the method of analysing the volcanic response by averaging the response over the 2 winters post-eruption, which has been used in several studies previously mentioned, might be masking this stronger response in the first year. This stronger initial response was seen in all fields investigated except for the jet speed index used, and the patterns were consistent with those expected of a positive NAO phase when looking at the entire period of regression from 1900-2010 (or 1870-2010 for certain datasets). This positive NAO phase and the associated response patterns in the first winter appear consistent with mechanisms proposed involving the strengthening of the polar vortex due to equatorial stratospheric heating caused by large eruptions.

Investigating slightly shorter time periods centred around certain eruptions shows that the strongest responses in all fields seemed to be coming from the most recent time period from 1980-2010, which includes the eruptions of El Chichón in 1982 and Pinatubo in 1991, both of which were very large. This pattern appears to dominate when looking at the whole period. In contrast, it seems that the period from 1950-1980 centred on the Agung eruption in 1963 shows an almost opposite pattern of responses, indicative more of a negative NAO phase in the first winter.

Furthermore, looking at a lagged response showing the first six years following an eruption shows an apparent 'lag 4 response' pattern, which shows statistical significance in several fields (SLP, SST, jet speed, and blocking), and is in fact the only significant response seen in the jet speed index which showed no initial response. This 'lag 4 response' pattern shows almost a reversal in the response pattern of the first winter, i.e. where the initial response was a positive NAO phase pattern, at lag 4 it shows something more similar to a negative NAO phase. This is something that would benefit from some further study to determine whether there is a physical mechanism at play here, possibly involving the oceans as effects can persist over a longer timescale there, or whether this response keeps appearing as an artefact of the regression method. It is hard to make a firm conclusion on this at this point, however the fact that this appears in several (but not all) of the fields looked at here, as well as in one part of the jet indices (the jet speed) and not the other (the jet latitude) does suggest that there may be an underlying mechanism causing this response, and possibly further implies different mechanisms influencing different aspects of the North Atlantic jet. Previous studies have looked into the impact of eruptions on the oceans and found several effects at lags longer than one or two years (as discussed in Section 2.2.6) which could support a mechanism involving the oceans leading to this 'lag 4 response'.

5.1 Further Work

The work presented here has revealed some potentially interesting results that would certainly warrant some further investigation. As mentioned in the previous sub-section, this 'lag 4 response' pattern is one of them. Being able to determine whether this is real or not would be very useful, and if this does prove to be a real response investigating a potential mechanism to describe this response would be very interesting. Looking at extended lags up to 10 or even 30 years following an eruption could be useful here to investigate potential mechanisms involving the oceans, which as mentioned before allow effects to persist for longer timescales. Further statistical testing, for example testing field significance, could also be carried out on these results to try to determine the validity of the lag 4 response.

Another result that could be interesting to look into further is the apparently different response to the Agung eruption compared to other large eruptions, particularly Pinatubo or El Chichón. This was shown when looking at shorter regression time periods. Simply taking a quick look at the background conditions at the time of these eruptions, for example the ENSO phase, and comparing those doesn't show anything obviously different about the Agung eruption. These are shown in Table 1 (Section 3). All three eruptions show an El Niño phase in the first winter, for example, and are at similar stages in the AMO cycle. The QBO phase at the time of the eruptions of Agung and Pinatubo are opposite, however the QBO at the time of the El Chichón eruption is the same as during Agung. The QBO phase has been shown to have potential influences on the response of a volcanic eruption, as discussed in Section 2.2.4, so this could be a possible factor for the differing responses and could be investigated. Also, simply looking at the spatial distribution of the volcanic aerosol following the eruptions could shed light on some differences – it can be seen from Figure 6 for example that most of the aerosols from the Agung eruption seem to be concentrated in the Southern Hemisphere, whereas that of El Chichón is mostly in the Northern Hemisphere, and for Pinatubo it was distributed across both

hemispheres. The influence of these background conditions could be investigated using some model simulations which simulate the response from specific eruptions represented by injections of aerosols in a certain region or forced temperature anomalies at different points in the stratosphere. The background conditions themselves could be experimented with, for example running experiments with certain sources of variability removed, or by nudging some of the fields towards different states to see whether the tropospheric or surface response changes. It could also be interesting to see whether the surface impacts were influenced by the fact that the Pinatubo eruption occurred only nine years after the eruption of El Chichón, which was also fairly large, which might have allowed the impacts to accumulate, compared to Agung which occurred after about a 50-year period with no large eruptions.

Similar modelling simulation experiments could be performed to gain a more in depth understanding of the physical mechanisms that are at play when looking at the response to volcanic eruptions. For example, different SSTs could be imposed in different model runs to see whether the surface cooling is important to the NAO and jet response. The influence of the polar vortex could also be examined further, for example by nudging the polar vortex to a different state to see if the mechanism involving the polar vortex response is critical to the existence of the tropospheric and surface response, or if the effect of the lower stratospheric temperature gradient change on synoptic scale waves is more important. Investigating the stratospheric circulation in reanalysis data could also shed some light on possible mechanisms, particularly for the most recent period which seems to dominate the volcanic responses and also has reasonable representation of the stratosphere in available reanalyses.

Finally, it would also be interesting to investigate the impact of volcanic eruptions using CMIP6 data, which is now available, and compare this to the results from the CMIP5 data to see whether the representation of volcanic eruptions has improved in climate model simulations or

not. This could be done using a similar composite analysis to previous studies which looked at CMIP5 data (e.g. Driscoll et al., 2012) and also using the regression analysis method used here.

References:

Adams, J.B., Mann, M.E. and Ammann, C.M., 2003. Proxy evidence for an El Nino-like response to volcanic forcing. *Nature*, *426*(6964), p.274.

Allan, R. and Ansell, T., 2006. A new globally complete monthly historical gridded mean sea level pressure dataset (HadSLP2): 1850–2004. *Journal of Climate*, *19*(22), pp.5816-5842.

Apel, J.R. 1987. Principles of Ocean Physics. London: Academic.

Baldwin, M.P. and Dunkerton, T.J., 1999. Propagation of the Arctic Oscillation from the stratosphere to the troposphere. *Journal of Geophysical Research: Atmospheres*, *104*(D24), pp.30937-30946.

Baldwin, M.P. and Dunkerton, T.J., 2001. Stratospheric harbingers of anomalous weather regimes. *Science*, *294*(5542), pp.581-584.

Balmaseda, M.A., Trenberth, K.E. and Källén, E., 2013. Distinctive climate signals in reanalysis of global ocean heat content. *Geophysical Research Letters*, *40*(9), pp.1754-1759.

Bittner, M., Schmidt, H., Timmreck, C. and Sienz, F., 2016. Using a large ensemble of simulations to assess the Northern Hemisphere stratospheric dynamical response to tropical volcanic eruptions and its uncertainty. *Geophysical Research Letters*, *43*(17), pp.9324-9332.

Bluth, G.J., Doiron, S.D., Schnetzler, C.C., Krueger, A.J. and Walter, L.S., 1992. Global tracking of the SO2 clouds from the June, 1991 Mount Pinatubo eruptions. *Geophysical Research Letters*, *19*(2), pp.151-154.

Brewer, A.W., 1949. Evidence for a world circulation provided by the measurements of helium and water vapour distribution in the stratosphere. *Quarterly Journal of the Royal Meteorological Society*, *75*(326), pp.351-363.

Butchart, N., 2014. The Brewer-Dobson circulation. *Reviews of geophysics*, *52*(2), pp.157-184.

Charney, J.G. and Drazin, P.G., 1961. Propagation of planetary-scale disturbances from the lower into the upper atmosphere. *Journal of Geophysical Research*, *66*(1), pp.83-109.

Chiodo, G., Marsh, D.R., Garcia-Herrera, R., Calvo, N. and García, J.A., 2014. On the detection of the solar signal in the tropical stratosphere. *Atmospheric Chemistry and Physics*, *14*(11), pp.5251-5269.

Compo, G.P., Whitaker, J.S., Sardeshmukh, P.D., Matsui, N., Allan, R.J., Yin, X., Gleason, B.E., Vose, R.S., Rutledge, G., Bessemoulin, P. and Brönnimann, S., 2011. The twentieth century reanalysis project. *Quarterly Journal of the Royal Meteorological Society*, *137*(654), pp.1-28.

Crooks, S.A. and Gray, L.J., 2005. Characterization of the 11-year solar signal using a multiple regression analysis of the ERA-40 dataset. *Journal of Climate*, *18*(7), pp.996-1015.

DallaSanta, K., Gerber, E.P. and Toohey, M., 2019. The circulation response to volcanic eruptions: The key roles of stratospheric warming and eddy interactions. *Journal of Climate*, *32*(4), pp.1101-1120.

Delworth, T.L. and Dixon, K.W., 2000. Implications of the recent trend in the Arctic/North Atlantic Oscillation for the North Atlantic thermohaline circulation. *Journal of Climate*, *13*(21), pp.3721-3727.

Dessler, A., 2000. *Chemistry and Physics of stratospheric ozone* (Vol. 74). Academic press.

Ding, Y., Carton, J.A., Chepurin, G.A., Stenchikov, G., Robock, A., Sentman, L.T. and Krasting, J.P., 2014. Ocean response to volcanic eruptions in Coupled Model Intercomparison Project 5 simulations. *Journal of Geophysical Research: Oceans*, *119*(9), pp.5622-5637.

Dobson, G.M.B., 1956. Origin and distribution of the polyatomic molecules in the atmosphere. *Proceedings of the Royal Society of London. Series A. Mathematical and Physical Sciences*, *236*(1205), pp.187-193.

Driscoll, S., Bozzo, A., Gray, L.J., Robock, A. and Stenchikov, G., 2012. Coupled Model Intercomparison Project 5 (CMIP5) simulations of climate following volcanic eruptions. *Journal of Geophysical Research: Atmospheres*, *117*(D17).

Emile-Geay, J., Seager, R., Cane, M.A., Cook, E.R. and Haug, G.H., 2008. Volcanoes and ENSO over the past millennium. *Journal of Climate*, *21*(13), pp.3134-3148.

Enfield, D.B., Mestas-Nuñez, A.M. and Trimble, P.J., 2001. The Atlantic multidecadal oscillation and its relation to rainfall and river flows in the continental US. *Geophysical Research Letters*, *28*(10), pp.2077-2080.

Fujiwara, M., Hibino, T., Mehta, S.K., Gray, L., Mitchell, D. and Anstey, J., 2015. Global temperature response to the major volcanic eruptions in multiple reanalysis data sets. *Atmospheric chemistry and physics*, *15*(23), pp.13507-13518.

Fujiwara, M., Wright, J.S., Manney, G.L., Gray, L.J., Anstey, J., Birner, T., Davis, S., Gerber, E.P., Harvey, V.L., Hegglin, M.I. and Homeyer, C.R., 2017. Introduction to the SPARC Reanalysis Intercomparison Project (S-RIP) and overview of the reanalysis systems. *Atmospheric Chemistry and Physics*, *17*(2), pp.1417-1452.

Fujiwara, M., Martineau, P. and Wright, J.S., 2020. Surface temperature response to the major volcanic eruptions in multiple reanalysis data sets. *Atmospheric Chemistry and Physics*, *20*(1), pp.345-374.

Gao, C., Robock, A. and Ammann, C., 2008. Volcanic forcing of climate over the past 1500 years: An improved ice core-based index for climate models. *Journal of Geophysical Research: Atmospheres*, *113*(D23).

Gerber, E.P. and Martineau, P., 2018. Quantifying the variability of the annular modes: reanalysis uncertainty vs. sampling uncertainty. Atmospheric Chemistry and Physics, 18(23), pp.17099-17117.

Gray, L.J., Scaife, A.A., Mitchell, D.M., Osprey, S., Ineson, S., Hardiman, S., Butchart, N., Knight, J., Sutton, R. and Kodera, K., 2013. A lagged response to the 11 year solar cycle in observed winter Atlantic/European weather patterns. *Journal of Geophysical Research: Atmospheres*, *118*(24).

Gray, L.J., Woollings, T.J., Andrews, M. and Knight, J., 2016. Eleven-year solar cycle signal in the NAO and Atlantic/European blocking. *Quarterly Journal of the Royal Meteorological Society*, *142*(698), pp.1890-1903.

GROISMAN, P., 1985. Regional climatic consequences of volcanic eruptions. *Meteorologiia I Gidrologiia*, pp.39-45.

Grumbine, R. W., 1996. Automated passive microwave sea ice concentration analysis at NCEP, NCEP/OMB Technical Note No. 121, NCEP Environmental Modeling Center, Camp Springs, Maryland, 13 pp., 1996.

Hirono, M., 1988. On the trigger of El Niño Southern Oscillation by the forcing of early El Chichón volcanic aerosols. *Journal of Geophysical Research: Atmospheres*, *93*(D5), pp.5365-5384.

Hoinka, K.P., 1999. Temperature, humidity, and wind at the global tropopause. *Monthly Weather Review*, *127*(10), pp.2248-2265.

Holton, J.R., 1992. *An Introduction to Dynamical Meteorology* (3rd Edition), Academic Press

Holton, J.R. and Tan, H.C., 1982. The quasi-biennial oscillation in the Northern Hemisphere lower stratosphere. *Journal of the Meteorological Society of Japan. Ser. II*, *60*(1), pp.140-148.

Holton, J.R., Haynes, P.H., McIntyre, M.E., Douglass, A.R., Rood, R.B. and Pfister, L., 1995. Stratosphere-troposphere exchange. *Reviews of geophysics*, *33*(4), pp.403-439.

Hurrell, J.W., Kushnir, Y., Ottersen, G., Visbeck, M., 2003. An overview of the north atlantic oscillation. *The North Atlantic Oscillation: Climatic Significance and Environmental Impact*. American Geophysical Union (AGU), pp. 1–35

Jones, P.D., Jonsson, T. and Wheeler, D., 1997. Extension to the North Atlantic Oscillation using early instrumental pressure observations from Gibraltar and South-West Iceland. *International Journal of climatology*, *17*(13), pp.1433-1450.

Kalnay, E., Kanamitsu, M., Kistler, R., Collins, W., Deaven, D., Gandin, L., Iredell, M., Saha, S., White, G., Woollen, J. and Zhu, Y., 1996. The NCEP/NCAR 40-year reanalysis project. Bulletin of the American meteorological Society, 77(3), pp.437-472.

Kidston, J., Scaife, A.A., Hardiman, S.C., Mitchell, D.M., Butchart, N., Baldwin, M.P. and Gray, L.J., 2015. Stratospheric influence on tropospheric jet streams, storm tracks and surface weather. *Nature Geoscience*, *8*(6), p.433.

Kniskern, F.E., 1991. The Navy/NOAA Joint Ice Center's role in the climate and global change program. *Global and Planetary Change*, *4*(1-3), pp.207-212.

Kodera, K., 1994. Influence of volcanic eruptions on the troposphere through stratospheric dynamical processes in the Northern Hemisphere winter. *Journal of Geophysical Research: Atmospheres*, *99*(D1), pp.1273-1282.

Lamb, H.H., 1970. Volcanic dust in the atmosphere; with a chronology and assessment of its meteorological significance. *Philosophical Transactions of the Royal Society of London A: Mathematical, Physical and Engineering Sciences*, *266*(1178), pp.425-533.

Lehner, F., Schurer, A.P., Hegerl, G.C., Deser, C. and Frölicher, T.L., 2016. The importance of ENSO phase during volcanic eruptions for detection and attribution. *Geophysical Research Letters*, *43*(6), pp.2851-2858.

Mitchell, J.M., 1970. A preliminary evaluation of atmospheric pollution as a cause of the global temperature fluctuation of the past century. In *Global effects of environmental pollution* (pp. 139-155). Springer, Dordrecht.

Mitchell, D.M., Gray, L.J., Anstey, J., Baldwin, M.P. and Charlton-Perez, A.J., 2013. The influence of stratospheric vortex displacements and splits on surface climate. *Journal of Climate*, *26*(8), pp.2668-2682.

Mitchell, D.M., Gray, L.J., Fujiwara, M., Hibino, T., Anstey, J.A., Ebisuzaki, W., Harada, Y., Long, C., Misios, S., Stott, P.A. and Tan, D., 2015. Signatures of naturally induced variability in the atmosphere using multiple reanalysis datasets. *Quarterly Journal of the Royal Meteorological Society*, *141*(691), pp.2011-2031.

Newhall, C.G. and Self, S., 1982. The volcanic explosivity index (VEI) an estimate of explosive magnitude for historical volcanism. *Journal of Geophysical Research: Oceans*, *87*(C2), pp.1231-1238.

Otterå, O.H., Bentsen, M., Drange, H. and Suo, L., 2010. External forcing as a metronome for Atlantic multidecadal variability. *Nature Geoscience*, *3*(10), p.688.

Parker, D. E., Folland, C. K., Bevan, A., Ward, M. N., Jackson, M., and Maskell, K., 1995. Marine surface data for analysis of climatic fluctuations on interannual to century time scales. *Natural Climate Variability on Decade-to-Century Time Scales*, edited by: Martinson, D. G., Bryan, K., Ghil, M., Hall, M. M., Karl, T. R., Sarachik, E. S., Sorooshian, S., and Talley, L. D., National Academic Press, Washington, D.C., pp.241–250.

Poli, P., Hersbach, H., Dee, D.P., Berrisford, P., Simmons, A.J., Vitart, F., Laloyaux, P., Tan, D.G., Peubey, C., Thépaut, J.N. and Trémolet, Y., 2016. ERA-20C: An atmospheric reanalysis of the twentieth century. Journal of Climate, 29(11), pp.4083-4097.

Rayner, N.A.A., Parker, D.E., Horton, E.B., Folland, C.K., Alexander, L.V., Rowell, D.P., Kent, E.C. and Kaplan, A., 2003. Global analyses of sea surface temperature, sea ice, and night marine air temperature since the late nineteenth century. *Journal of Geophysical Research: Atmospheres*, *108*(D14).

Reynolds, R.W. and Smith, T.M., 1994. Improved global sea surface temperature analyses using optimum interpolation. *Journal of climate*, *7*(6), pp.929-948.

Robock, A., 2000. Volcanic eruptions and climate. *Reviews of Geophysics*, *38*(2), pp.191-219.

Robock, A. and Mass, C., 1982. The Mount St. Helens volcanic eruption of 18 May 1980: Large short-term surface temperature effects. *Science*, *216*(4546), pp.628-630.

Robock, A. and Mao, J., 1992. Winter warming from large volcanic eruptions. *Geophysical Research Letters*, *19*(24), pp.2405-2408.

Robock, A. and Free, M.P., 1995. Ice cores as an index of global volcanism from 1850 to the present. *Journal of Geophysical Research: Atmospheres*, *100*(D6), pp.11549-11567.

Robock, A., Taylor, K.E., Stenchikov, G.L. and Liu, Y., 1995. GCM evaluation of a mechanism for El Niño triggering by the El Chichón ash cloud. *Geophysical research letters*, *22*(17), pp.2369-2372.

Sato, M., Hansen, J.E., McCormick, M.P. and Pollack, J.B., 1993. Stratospheric aerosol optical depths, 1850–1990. *Journal of Geophysical Research: Atmospheres*, *98*(D12), pp.22987-22994.

Scherrer, S.C., Croci-Maspoli, M., Schwierz, C. and Appenzeller, C., 2006. Two-dimensional indices of atmospheric blocking and their statistical relationship with winter climate patterns in the Euro-Atlantic region. *International Journal of Climatology: A Journal of the Royal Meteorological Society*, *26*(2), pp.233-249.

Self, S., Rampino, M.R., Zhao, J. and Katz, M.G., 1997. Volcanic aerosol perturbations and strong El Nino events: No general correlation. *Geophysical Research Letters*, *24*(10), pp.1247-1250.

Shindell, D.T., Schmidt, G.A., Miller, R.L. and Mann, M.E., 2003. Volcanic and solar forcing of climate change during the preindustrial era. *Journal of Climate*, *16*(24), pp.4094-4107.

Simkin, T., Siebert, L., McClelland, L., Bridge, D., Newhall, C. and Latter, J.H., 1981. *Volcanoes of the world: a regional directory, gazetteer, and chronology of volcanism during the last 10,000 years*. US Hutchinson Ross Publishing.

Simpson, I.R., Blackburn, M. and Haigh, J.D., 2009. The role of eddies in driving the tropospheric response to stratospheric heating perturbations. *Journal of the Atmospheric Sciences*, *66*(5), pp.1347-1365.

Soden, B.J., Wetherald, R.T., Stenchikov, G.L. and Robock, A., 2002. Global cooling after the eruption of Mount Pinatubo: A test of climate feedback by water vapor. *science*, *296*(5568), pp.727-730.

Stenchikov, G.L., Kirchner, I., Robock, A., Graf, H.F., Antuna, J.C., Grainger, R.G., Lambert, A. and Thomason, L., 1998. Radiative forcing from the 1991 Mount Pinatubo volcanic eruption. *Journal of Geophysical Research: Atmospheres*, *103*(D12), pp.13837-13857.

Stenchikov, G., Hamilton, K., Robock, A., Ramaswamy, V. and Schwarzkopf, M.D., 2004. Arctic oscillation response to the 1991 Pinatubo eruption in the SKYHI general circulation model with a realistic quasi-biennial oscillation. *Journal of Geophysical Research: Atmospheres*, *109*(D3).

Stenchikov, G., Hamilton, K., Stouffer, R.J., Robock, A., Ramaswamy, V., Santer, B. and Graf, H.F., 2006. Arctic Oscillation response to volcanic eruptions in the IPCC AR4 climate models. *Journal of Geophysical Research: Atmospheres*, *111*(D7).

Stenchikov, G., Delworth, T.L., Ramaswamy, V., Stouffer, R.J., Wittenberg, A. and Zeng, F., 2009. Volcanic signals in oceans. *Journal of Geophysical Research: Atmospheres*, *114*(D16).

Stocker, M., Ladstädter, F., Wilhelmsen, H. and Steiner, A.K., 2019. Quantifying Stratospheric Temperature Signals and Climate Imprints From Post-2000 Volcanic Eruptions. *Geophysical research letters*, *46*(21), pp.12486-12494.

Stowe, L.L., Carey, R.M. and Pellegrino, P.P., 1992. Monitoring the Mt. Pinatubo aerosol layer with NOAA/11 AVHRR data. *Geophysical research letters*, *19*(2), pp.159-162.

Strong, A.E., 1984. Monitoring El Chichón aerosol distribution using NOAA-7 satellite AVHRR sea surface temperature observations. *Geofisica Internacional*, *23*(2).159-162.

Swingedouw, D., Mignot, J., Ortega, P., Khodri, M., Menegoz, M., Cassou, C. and Hanquiez, V., 2017. Impact of explosive volcanic eruptions on the main climate variability modes. *Global and Planetary Change*, *150*, pp.24-45.

Symons, G.J. ed., 1888. *The Eruption of Krakatoa, and Subsequent Phenomena: Report of the Krakatoa Committee of the Royal Society*. London: Trübner.

Thomas, M.A., Giorgetta, M.A., Timmreck, C., Graf, H.F. and Stenchikov, G., 2009. Simulation of the climate impact of Mt. Pinatubo eruption using ECHAM5–Part 2: Sensitivity to the phase of the QBO and ENSO. *Atmospheric Chemistry and Physics*, *9*(9), pp.3001-3009.

Timmreck, C., 2012. Modeling the climatic effects of large explosive volcanic eruptions. *Wiley Interdisciplinary Reviews: Climate Change*, *3*(6), pp.545-564.

Titchner, H.A. and Rayner, N.A., 2014. The Met Office Hadley Centre sea ice and sea surface temperature data set, version 2: 1. Sea ice concentrations. *Journal of Geophysical Research: Atmospheres*, *119*(6), pp.2864-2889.

Toohey, M., Krüger, K., Bittner, M., Timmreck, C. and Schmidt, H., 2014. The impact of volcanic aerosol on the Northern Hemisphere stratospheric polar vortex: mechanisms and sensitivity to forcing structure. *Atmospheric Chemistry and Physics*, *14*(23), pp.13063-13079.

Trenberth, K.E. and Dai, A., 2007. Effects of Mount Pinatubo volcanic eruption on the hydrological cycle as an analog of geoengineering. *Geophysical Research Letters*, *34*(15).

Vernier, J.P., Thomason, L.W., Pommereau, J.P., Bourassa, A., Pelon, J., Garnier, A., Hauchecorne, A., Blanot, L., Trepte, C., Degenstein, D. and Vargas, F., 2011. Major influence of tropical volcanic eruptions on the stratospheric aerosol layer during the last decade. *Geophysical Research Letters*, *38*(12).

Waugh, D.W. and Polvani, L.M., 2010. Stratospheric polar vortices. *The Stratosphere: Dynamics, Transport, and Chemistry, Geophys. Monogr., Vol. 190, Amer. Geophys. Union*, 43–57.

Waugh, D.W., Sobel, A.H. and Polvani, L.M., 2017. What is the polar vortex and how does it influence weather?. *Bulletin of the American Meteorological Society*, *98*(1), pp.37-44.

Wilson, R., Cook, E., D'Arrigo, R., Riedwyl, N., Evans, M.N., Tudhope, A. and Allan, R., 2010. Reconstructing ENSO: the influence of method, proxy data, climate forcing and teleconnections. *Journal of Quaternary Science*, *25*(1), pp.62-78.

Woollings, T., Hoskins, B., Blackburn, M. and Berrisford, P., 2008. A new Rossby wave–breaking interpretation of the North Atlantic Oscillation. *Journal of the Atmospheric Sciences*, *65*(2), pp.609-626.

Woollings, T., Hannachi, A. and Hoskins, B., 2010a. Variability of the North Atlantic eddy-driven jet stream. *Quarterly Journal of the Royal Meteorological Society*, *136*(649), pp.856-868.

Woollings, T., Charlton-Perez, A., Ineson, S., Marshall, A.G. and Masato, G., 2010b. Associations between stratospheric variability and tropospheric blocking. *Journal of Geophysical Research: Atmospheres*, *115*(D6).

Woollings, T., Czuchnicki, C. and Franzke, C., 2014. Twentieth century North Atlantic jet variability. *Quarterly Journal of the Royal Meteorological Society*, *140*(680), pp.783-791.

Woollings, T., Franzke, C., Hodson, D.L.R., Dong, B., Barnes, E.A., Raible, C.C. and Pinto, J.G., 2015. Contrasting interannual and multidecadal NAO variability. *Climate dynamics*, *45*(1-2), pp.539-556.

Wunderlich, F. and Mitchell, D.M., 2017. Revisiting the observed surface climate response to large volcanic eruptions. *Atmospheric Chemistry and Physics*, *17*(1), pp.485-499.

Zanchettin, D., Bothe, O., Graf, H.F., Lorenz, S.J., Luterbacher, J., Timmreck, C. and Jungclaus, J.H., 2013a. Background conditions influence the decadal climate response to strong volcanic eruptions. *Journal of Geophysical Research: Atmospheres*, *118*(10), pp.4090-4106.

Zanchettin, D., Timmreck, C., Bothe, O., Lorenz, S.J., Hegerl, G., Graf, H.F., Luterbacher, J. and Jungclaus, J.H., 2013b. Delayed winter warming: A robust decadal response to strong tropical volcanic eruptions?. *Geophysical Research Letters*, *40*(1), pp.204-209.

Zebiak, S.E. and Cane, M.A., 1987. A Model El Niñ–Southern Oscillation. *Monthly Weather Review*, *115*(10), pp.2262-2278.